Pergamon

Geochimica et Cosmochimica Acta, Vol. 67, No. 21, pp. 4205–4221, 2003

0016-7037/03 $30.00 + .00

doi:10.1016/S0016-7037(03)00277-1

CaO-MgO-Al_2O_3-SiO_2 liquids: Chemical and isotopic effects of Mg and Si evaporation in a closed system of solar composition

L. GROSSMAN[1,2,*] and A. V. FEDKIN[1]

[1]Department of the Geophysical Sciences, The University of Chicago, 5734 S. Ellis Ave., Chicago, IL 60637, USA
[2]The Enrico Fermi Institute, The University of Chicago, 5640 S. Ellis Ave., Chicago, IL 60637, USA

(*Received November* 22, 2002; *accepted in revised form March* 7, 2003)

Abstract—A method is shown for calculating vapor pressures over a CMAS droplet in a gas of any composition. It is applied to the problem of the evolution of the chemical and Mg and Si isotopic composition of a completely molten droplet having the composition of a likely refractory inclusion precursor during its evaporation into the complementary, i.e. modified solar, gas from which it originally condensed, a more realistic model than previous calculations in which the ambient gas is pure $H_{2(g)}$. Because the loss rate of Mg is greater than that of Si, the vapor pressure of $Mg_{(g)}$ falls and its ambient pressure rises faster than those of $SiO_{(g)}$ during isothermal evaporation, causing the flux of $Mg_{(g)}$ to approach zero faster and MgO to approach its equilibrium concentration sooner than SiO_2. As time passes, δ^{25}Mg and δ^{29}Si increase in the droplet and decrease in the ambient gas. The net flux of each isotope crossing the droplet/gas interface is the difference between its outgoing and incoming flux. δ^{25}Mg and δ^{29}Si of this instantaneous gas become higher, first overtaking their values in the ambient gas, causing them to increase with time, and later overtaking their values in the droplet itself, causing them to decrease with time, ultimately reaching their equilibrium values. If the system is cooling during evaporation and if mass transfer ceases at the solidus temperature, 1500 K, final MgO and SiO_2 contents of the droplet are slightly higher in modified solar gas than in pure $H_{2(g)}$, and the difference increases with decreasing cooling rate and increasing ambient pressure. During cooling under some conditions, net fluxes of evaporating species become negative, causing reversal of the evaporation process into a condensation process, an increase in the MgO and/or SiO_2 content of the droplet with time, and an increase in their final concentrations with increasing ambient pressure and/or dust/gas ratio. At cooling rates $<\sim$3 K/h, closed-system evaporation at $P^{tot} \sim 10^{-3}$ bar in a modified solar gas, or at lower pressure in systems with enhanced dust/gas ratio, can yield the same δ^{25}Mg in a residual CMAS droplet for vastly different evaporated fractions of Mg. The δ^{25}Mg of a refractory residue may thus be insufficient to determine the extent of Mg loss from its precursor. Evaporation of Mg into an Mg-bearing ambient gas causes δ^{26}Mg and δ^{25}Mg of the residual droplet to fall below values expected from Rayleigh fractionation for the amount of ^{24}Mg evaporated, with the degree of departure increasing with increasing fraction evaporated and ambient pressure of Mg. δ^{26}Mg and δ^{25}Mg do not depart proportionately from Rayleigh fractionation curves, with δ^{25}Mg being less than expected on the basis of δ^{26}Mg by up to $\sim$1.2‰. Such departures from Rayleigh fractionation could be used in principle to distinguish heavily from lightly evaporated residues with the same δ^{25}Mg.

1. INTRODUCTION

Vapor-condensed phase fractionation processes are acknowledged to have played a critical role in determining chemical differences between different types of inclusions in chondritic meteorites, between the different classes of chondrites themselves and between the terrestrial planets. Although equilibrium condensation processes in the solar nebula have been investigated theoretically in great detail (e.g., Ebel and Grossman, 2000), theoretical treatment of evaporation kinetics is, by comparison, in its infancy.

Grossman et al. (2000) suggested that refractory inclusions in CV3 chondrites formed by melting of high-temperature condensate assemblages, followed by partial volatilization of Mg and Si from the liquids so formed. In so doing, they developed techniques for calculating the vapor pressures of all species evaporating from a CaO-MgO-Al_2O_3-SiO_2 (CMAS) liquid into vacuum and into pure $H_{2(g)}$, and combined these with experimental data to compute the isothermal change in composition of such a droplet with progressive evaporation. This work was extended by Grossman et al. (2002) to take into account the simultaneous effects of crystallization and cooling rate on the change in chemical and isotopic composition during evaporation of a CMAS droplet. Because the ambient gas likely contained virtually all but the most refractory elements during evaporation of high-temperature condensates in the solar nebula, an important limitation of that work is the assumption that the surrounding gas contained only $H_{2(g)}$. Tsuchiyama et al. (1999) developed a technique for theoretical study of the evaporation rate of solid forsterite into a Mg- and Si-bearing solar nebular gas, and showed that the ambient gas suppresses δ^{26}Mg of the residue relative to that expected from the Rayleigh fractionation law. Humayun and Cassen (2000) predicted that isotope fractionation during evaporation of K into a K-containing gas would also deviate from Rayleigh fractionation. Ozawa and Nagahara (2001) developed a general model for computing chemical and isotopic fractionations due to isothermal evaporation of a binary mixture into an ambient gas containing the same elements, and also predicted isotopic fractionations that deviate from the Rayleigh law.

* Author to whom correspondence should be addressed (yosi@midway.uchicago.edu).

In this work, a technique is developed for calculating vapor pressures of all species over a CMAS droplet in a gas of any composition, and is used to compute chemical and isotopic changes in the droplet and coexisting gas due to closed-system evaporation during cooling at various rates. Some of this work was presented by Fedkin et al. (2002).

2. VAPOR PRESSURE

2.1. Method

2.1.1. Vapor pressures of chemical species

The driving force for evaporation is the difference in thermodynamic activity of a component between the droplet and the ambient gas. In this work, activities in the droplet are represented by equilibrium vapor pressures at the droplet surface computed from them, even though there may be no place where these vapor pressures can actually be measured. Once evaporation begins, there may be two contributors to the total amount of any element *i* present in the gas phase at the droplet surface, an amount originally present in the gas and an amount derived by evaporation. This can be expressed as

$$P_i^{\text{tot}} = P_i^{\text{gas}} + P_i^{\text{drop}}, \tag{1}$$

where P_i^{tot} is the total pressure of element *i* at the surface of the droplet, P_i^{gas} is the total initial, preevaporation pressure of element *i*, and P_i^{drop} is the evaporative contribution to the total pressure of element *i* at the droplet surface. For each element present only in the gas phase, H, He, C, N, P and S,

$$P_i^{\text{drop}} = 0 \tag{2}$$

and

$$P_i^{\text{tot}} = P_i^{\text{gas}}. \tag{3}$$

A value is assumed for $P_{\text{H}}^{\text{tot}}$, from which P_i^{gas} can be calculated for each element, given its atomic abundance, $A(i)$, relative to that of hydrogen, $A(\text{H})$, in the initial gas phase. For example,

$$P_{\text{C}}^{\text{gas}} = \frac{A(\text{C})\,P_{\text{H}}^{\text{tot}}}{A(\text{H})}. \tag{4}$$

A mass-balance equation is written for each element *i*, in which the sum of the partial pressures of all species of element *i*, multiplied by their respective stoichiometric coefficients, is equated to P_i^{tot}. As an example of the mass-balance equation for an element present only in the gas phase, that for nitrogen,

$$2P_{\text{N}_2} + P_{\text{NO}} + P_{\text{N}} + \cdots = P_{\text{N}}^{\text{gas}}, \tag{5}$$

is rewritten as

$$2K_1P_{\text{N}}^2 + K_2P_{\text{N}}P_{\text{O}} + P_{\text{N}} + \cdots = P_{\text{N}}^{\text{gas}}, \tag{6}$$

where K_1 and K_2 are the equilibrium constants for formation of $N_{2(g)}$ and $NO_{(g)}$, respectively, from their monatomic gaseous constituent elements. Elements present in both the gas and the liquid are Ca, Mg, Al, Si and O. In the mass-balance equation for each of these elements, such as that for magnesium,

$$P_{\text{Mg}} + P_{\text{MgO}} + \cdots = P_{\text{Mg}}^{\text{gas}} + P_{\text{Mg}}^{\text{drop}}, \tag{7}$$

the partial pressures of the species at the droplet surface are equal to their vapor pressures, so that the above equation is rewritten as

$$\frac{K_3a_{\text{MgO}}P_{\text{H}}^2}{P_{\text{H}_2\text{O}}} + K_4a_{\text{MgO}} + \cdots = P_{\text{Mg}}^{\text{gas}} + P_{\text{Mg}}^{\text{drop}}, \tag{8}$$

where K_3 and K_4 are the equilibrium constants for the volatilization reactions,

$$\text{MgO}_{(\text{l})} + 2\text{H}_{(\text{g})} \Leftrightarrow \text{Mg}_{(\text{g})} + \text{H}_2\text{O}_{(\text{g})} \tag{9}$$

and

$$\text{MgO}_{(\text{l})} \Leftrightarrow \text{MgO}_{(\text{g})}, \tag{10}$$

respectively, a_{MgO} is the activity of MgO in the liquid, and $P_{\text{H}_2\text{O}}$ and P_{H} are the partial pressures of $H_2O_{(g)}$ and $H_{(g)}$, respectively. The oxygen equation is a special case. In it, vapor pressure substitutions of the form of those in Eqn. 8 are made for the partial pressures of Ca-, Mg-, Al- and Si-containing species, and substitutions of the form of those in Eqn. 6 are made for the partial pressures of all other species. Because all equilibrium constants are fixed at a given temperature, and the activities of all liquid components are fixed at a given temperature and liquid composition, there are only 12 variables in the system, P_{H}, P_{He}, P_{C}, P_{N}, P_{O}, P_{P}, P_{S}, $P_{\text{O}}^{\text{drop}}$, $P_{\text{Mg}}^{\text{drop}}$, $P_{\text{Al}}^{\text{drop}}$, $P_{\text{Si}}^{\text{drop}}$, and $P_{\text{Ca}}^{\text{drop}}$. There is one mass-balance equation for each of the 11 elements, plus the following equation which expresses the fact that each metal atom that leaves the liquid must be accompanied in the gas by a number of oxygen atoms in stoichiometric proportion to it in its liquid oxide component,

$$P_{\text{O}}^{\text{drop}} = P_{\text{Ca}}^{\text{drop}} + P_{\text{Mg}}^{\text{drop}} + 1.5P_{\text{Al}}^{\text{drop}} + 2P_{\text{Si}}^{\text{drop}}. \tag{11}$$

The 47 most abundant gas species that form from these 11 elements in a system of solar composition were assumed to be present. Thermodynamic data were taken from the same database employed by Ebel and Grossman (2000), and the solar system elemental abundances from Anders and Grevesse (1989). Activities of the oxides in CMAS liquids as a function of temperature and composition were obtained from the model of Berman (1983). The equations were solved simultaneously to one part in 10^{31} using a method of successive approximations on an SGI Origin 2000 computer. The pressure so calculated of any Ca-, Mg-, Al- or Si-containing species is the vapor pressure of that species over a droplet of the specified composition at the specified temperature in a gas of specified composition and $P_{\text{H}}^{\text{tot}}$. The total pressure, P^{tot}, is the sum of the calculated pressures of all species.

2.1.2. Vapor pressures of isotopic species

Isotopic fractionations of Mg due to equilibrium effects are unknown. Here, equilibrium Mg isotopic fractionation between liquid and vapor is assumed to be zero. In this work, separate vapor pressures are calculated for $^{24}Mg_{(g)}$, $^{25}Mg_{(g)}$ and $^{26}Mg_{(g)}$ at each temperature by simply multiplying the vapor pressure of elemental Mg, P_{Mg}, by the abundance of each Mg isotope in the droplet, e.g., $P_{25}^{\text{vap}} = X_{25}P_{\text{Mg}}$, where P_{25}^{vap} is the vapor pressure of ^{25}Mg, and X_{25} is the abundance of ^{25}Mg as a fraction of the total Mg, defined such that $X_{24} + X_{25} + X_{26} = 1$.

Clayton et al. (1978) estimated reduced partition function ratios for forsterite and $SiO_{(g)}$ from which the $^{30}Si/^{28}Si$ ratio of forsterite would be expected to be 1.74, 1.99 and 2.31‰ higher than that of $SiO_{(g)}$ with which it is in equilibrium at 1500, 1400 and 1300 K, respectively. In this work, it is assumed that the silicon isotopic fractionation between SiO_2 in CMAS liquids and $SiO_{(g)}$ is the same as that between forsterite and $SiO_{(g)}$ at

the same temperature, and that there is no oxygen isotopic fractionation between these species. These fractionations were extrapolated quadratically in temperature, and used to compute the difference between the free energy of the evaporation reaction,

$$SiO_{2(l)} + 2H_{(g)} \Leftrightarrow SiO_{(g)} + H_2O_{(g)}, \quad (12)$$

for ^{30}Si and ^{28}Si in the temperature range of interest in this work. At 1700 K, for example, the free energy of Eqn. 12 is 20.48 J/mol more positive for ^{30}Si than for ^{28}Si. The difference in the free energy of Eqn. 12 between ^{29}Si and ^{28}Si is assumed to be half as much as that between ^{30}Si and ^{28}Si. In this work, separate vapor pressures are calculated for $^{30}SiO_{(g)}$, $^{29}SiO_{(g)}$ and $^{28}SiO_{(g)}$ at each temperature by using the different free energies of vaporization for each and assuming that the activity of each isotopic species of SiO_2 is equal to its isotopic abundance in the droplet multiplied by the activity of SiO_2 in the CMAS liquid. For example,

$$P^{vap}_{^{30}SiO} = K_{30} X_{30} a_{SiO_2} P^2_H / P_{H_2O}, \quad (13)$$

where $P^{vap}_{^{30}SiO}$ is the vapor pressure of $^{30}SiO_{(g)}$, K_{30} is the equilibrium constant for Eqn. 12 when all Si is ^{30}Si, $a_{S_iO_2}$ is the activity of SiO_2 in the droplet and X_{30} is the abundance of ^{30}Si as a fraction of the total Si, defined such that $X_{28} + X_{29} + X_{30} = 1$.

2.2. Vapor Pressures Over a CMAS Droplet in an Ambient Gas

Throughout this paper, the initial composition of the droplet is assumed to be that of δ, one of the condensate compositions preferred by Grossman et al. (2002) as a precursor of Allende Type B inclusions. It is the bulk chemical composition of the total equilibrium condensate assemblage calculated to form in a system of solar composition at 1313 K at a P^{tot} of 10^{-5} bar using the program of Ebel and Grossman (2000). It contains 24.37 wt.% CaO, 15.07% MgO, 30.79% Al_2O_3 and 29.77% SiO_2. Unless stated otherwise, it is further assumed throughout this paper that δ evaporates into its complementary gas, i.e., one having the bulk chemical composition of the gas that was in equilibrium with this condensate when it formed. This residual gas is referred to herein as modified solar gas, containing 7.03×10^{-5} of the solar abundance of Al, 2.3×10^{-4} of the Ca, 0.9304 of the Si, 0.9511 of the Mg, 0.9863 of the oxygen and 100% of the other seven elements assumed to be present in the system.

Imagine that a parcel of gas containing equilibrium proportions of condensate nodules of composition δ is heated and either compressed or expanded, causing melting and incipient evaporation of δ. Upon establishment of the vapor pressures of all species at the surface of any one of the droplets, the P_i^{drop}/P_i^{gas} ratio for Al, Ca, Mg, Si and O are those shown in Figures 1a, 1b, 1c, 1d, and 1e, respectively, as a function of the temperature and P_{H_2} of the new environment. For each element at constant P_{H_2}, the vapor at the surface of the droplet contains an increasing proportion of material derived from the droplet, and therefore a decreasing proportion of material originally present in the ambient gas, with increasing temperature. While the vapor pressures of most species generally increase with P_{H_2}, the partial pressures of most species in the ambient gas also generally increase in proportion to P_{H_2}, but at a faster rate. As a result, at constant temperature, the vapor at the surface of the droplet contains a decreasing proportion of material derived from the droplet with increasing P_{H_2}. Note that the ambient gas and the droplet contribute comparable amounts to the vapor at the surface of the droplet only at the lowest temperatures and highest values of P_{H_2} considered here. As shown in Figure 1 at 1500 K, for example, the proportions are equal for oxygen at $P_{H_2} \sim 1 \times 10^{-4}$ bar, for Si at $\sim 3 \times 10^{-4}$, for Mg at $\sim 3 \times 10^{-3}$, for Ca at $\sim 8 \times 10^{-3}$, and at much higher P_{H_2} for Al.

The actual vapor pressures of the most abundant species of Al, Ca, Mg, Si, and oxygen over δ at 1700 K are shown as a function of P_{H_2} in Figures 2a, 2b, 2c, 2d, and 2e, respectively. Just as in the case of evaporation into pure $H_{2(g)}$ (Grossman et al., 2000), the vapor pressures of all Ca- and Al-bearing species are much less than those of the most volatile Mg- and Si-bearing species, and the vapor pressures of the latter, $Mg_{(g)}$ and $SiO_{(g)}$, respectively, are much higher than those of all other Mg- and Si-bearing species. The functional relationships between the vapor pressures and P_{H_2} are almost identical to those seen in the earlier work. This is because of the fact that, even in a modified solar gas, the most favorable evaporation reactions for liquid metal oxides in a CMAS droplet are still those in which they react with hydrogen to form water, as in the redox Eqn. 9. At a given temperature, because the fO_2 over the droplet is only slightly higher (usually by 0.02–0.04 of a log unit) in modified solar gas than in pure $H_{2(g)}$ (Grossman et al., 2000), the vapor pressures of $Mg_{(g)}$ and $SiO_{(g)}$ are only slightly less in modified solar gas than in pure $H_{2(g)}$. The fO_2 at the surface of a droplet of composition δ immersed in modified solar gas is shown in Figure 3 as a function of P_{H_2} and temperature. Only at the lowest temperatures and highest values of P_{H_2} considered here does the log fO_2 at the surface of the evaporating droplet approach IW-6, that of the ambient solar gas.

In a theoretical study of forsterite evaporation in an ambient solar nebular gas, Tsuchiyama et al. (1999) discovered three evaporation regimes. In order of increasing P_{H_2}, they are the free evaporation-dominated regime, in which vapor pressures are virtually the same as in vacuum, and nearly independent of P_{H_2}; the hydrogen reaction-dominated regime, in which vapor pressures depend strongly on P_{H_2}; and the H_2O/H_2 buffer-dominated regime, in which vapor pressures again become independent of P_{H_2}, in this instance because the P_{H_2O}/P_{H_2} ratio is invariant with increasing P_{H_2}. It is because of this leveling off of vapor pressures in the latter regime that partial pressures in the ambient gas eventually overtake vapor pressures at high P_{H_2}. Another way of distinguishing the different regimes is that the ambient gas contributes neither hydrogen nor oxygen to the gas at the surface of the droplet in the free evaporation regime, the hydrogen and only a small fraction of the oxygen in the hydrogen reaction-dominated regime, and both the hydrogen and a preponderance of the oxygen in the H_2O/H_2 buffer-dominated regime. In Figure 3, note that log fO_2 becomes independent of P_{H_2} at the highest temperatures and lowest values of P_{H_2} because the gas composition is dominated by material evaporated from the droplet in the free evaporation regime. Tsuchiyama et al. (1999) solved analytical expressions for the vapor pressures in each regime by making different approximations in each, and smoothing the results in the transition regions between them. The advantage of the technique used here is that the same set of equations is solved precisely over the entire range of P_{H_2}. In this work, attention is restricted to a reasonable range of solar nebular values of P_{H_2} from 10^{-2} to 10^{-7} bar, almost

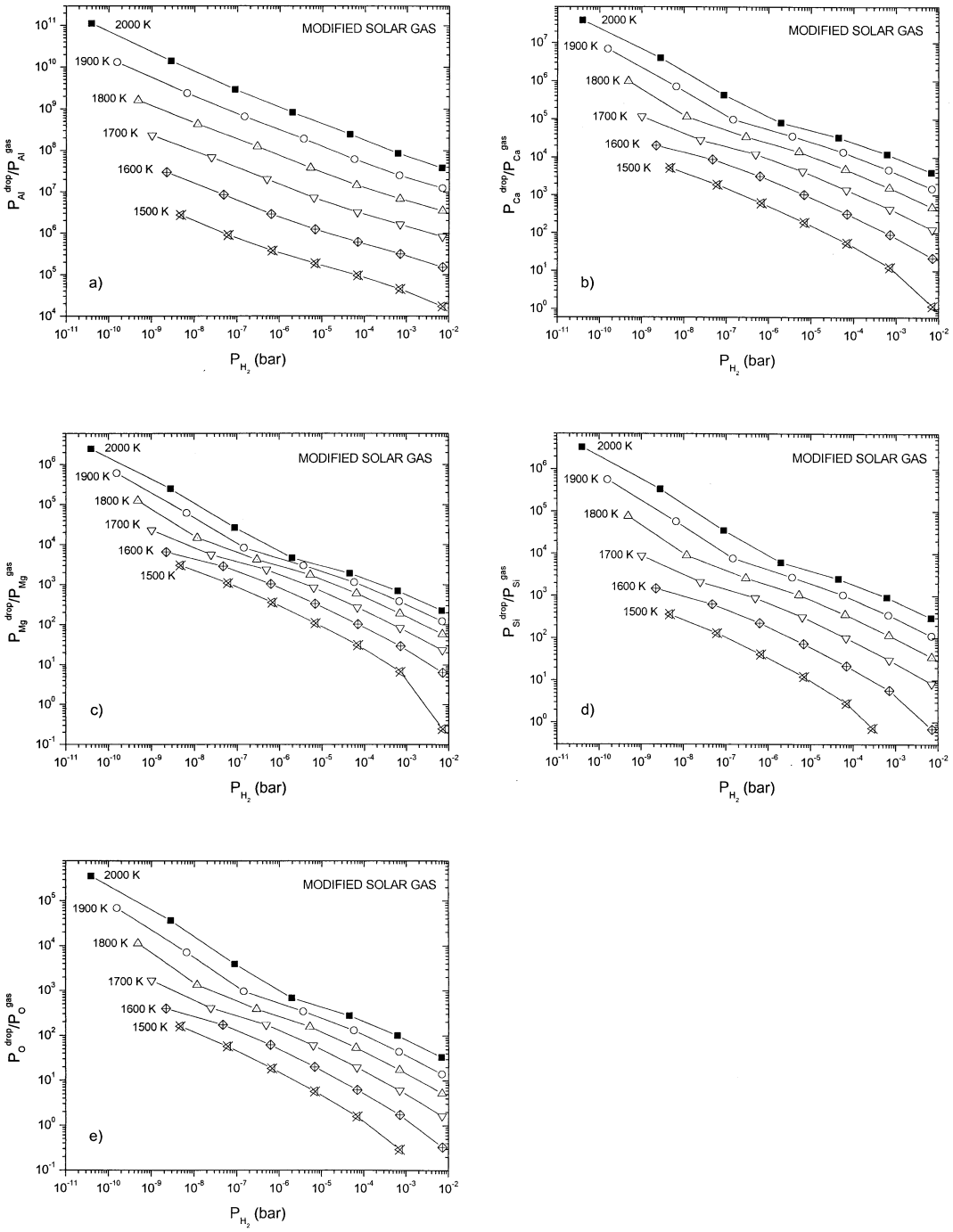

Fig. 1. Relative contribution of the amount of element *i* evaporated from a droplet of composition δ, P_i^{drop}, and the amount in the initial, modified solar gas, P_i^{gas}, to the vapor at the surface of the droplet for (a) aluminum; (b) calcium; (c) magnesium; (d) silicon; and (e) oxygen, plotted as a function of the partial pressure of H_2 for various temperatures.

entirely within the hydrogen reaction-dominated regime, as seen from the strong dependence of vapor pressures on P_{H_2} in Figure 2.

3. EVAPORATION RATE

3.1. Method

3.1.1. Elemental fluxes

Once the vapor pressure of a species is known over a droplet immersed in an ambient gas, the evaporation rate of that species into the ambient gas can be calculated using this form of the Hertz-Knudsen equation,

$$J_i = \frac{\alpha_i (P_i^{\mathrm{vap}} - P_i^{\mathrm{amb}})}{\sqrt{2\pi m_i RT}}, \tag{14}$$

where J_i, α_i and m_i are the net flux of evaporating molecules, the evaporation coefficient and the molecular weight, respectively, of species *i*, *R* is the gas constant and *T* the absolute

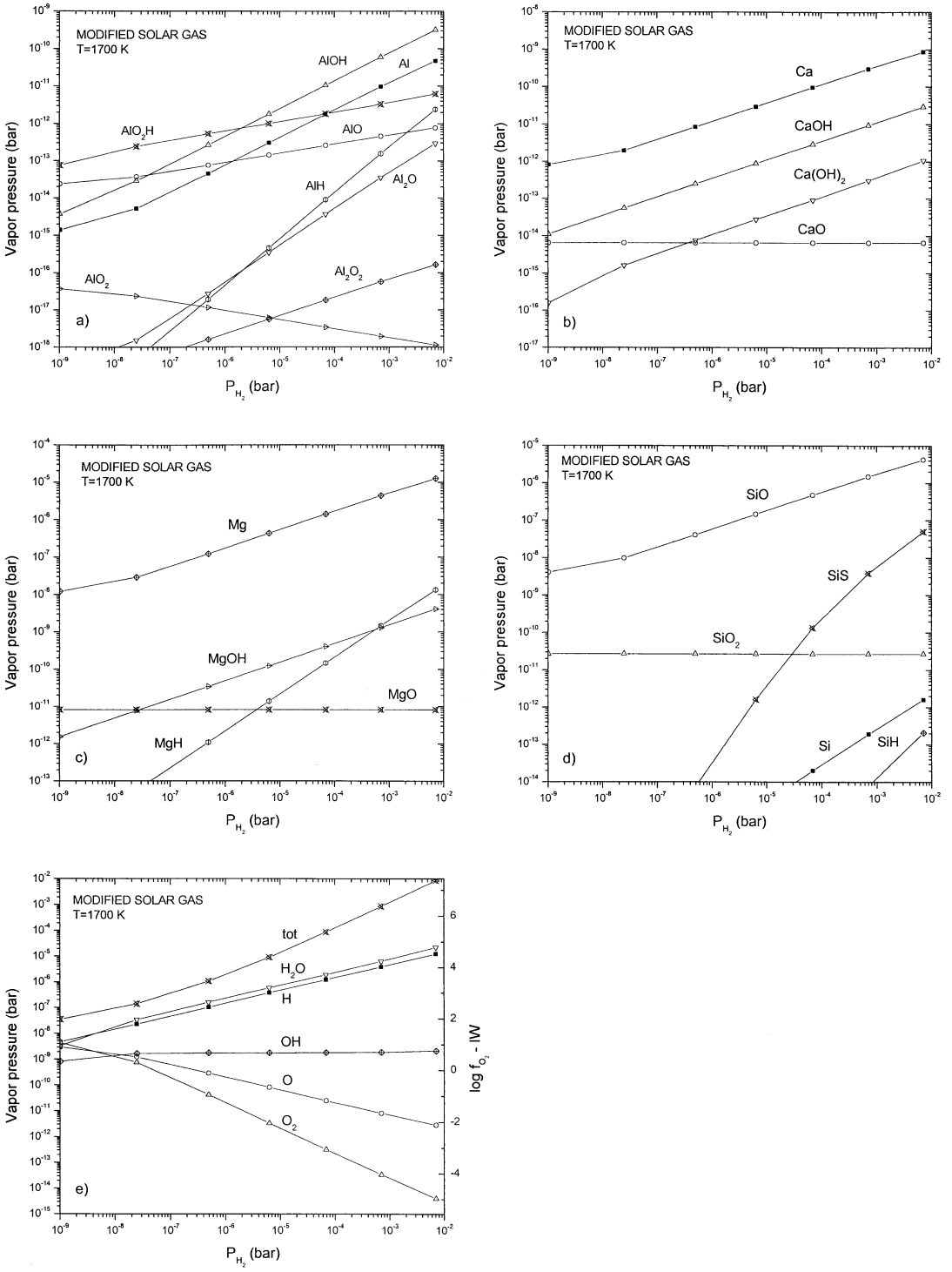

Fig. 2. Vapor pressures of the most abundant species over a droplet of composition δ in a modified solar gas at 1700 K for (a) aluminum; (b) calcium; (c) magnesium; (d) silicon; and (e) oxygen and hydrogen, plotted as a function of P_{H_2}. In (e), the partial pressure of O_2 is also expressed as a logarithm relative to the oxygen fugacity of the iron-wüstite (IW) buffer along the right margin. The variation of P^{tot} is also shown in (e).

temperature. P_i^{vap} is the vapor pressure of species *i* over the droplet as calculated above. P_i^{amb} is the partial pressure of species *i* in the ambient gas far enough away from the droplet that it is unconstrained by the oxide activities in the droplet. In this work, P_i^{amb} is obtained for all 47 species simultaneously at any P_H^{tot} and temperature by means of a pure gas-phase equilibrium calculation. In it, a mass-balance equation equivalent to Eqn. 5 and substitutions like those in Eqn. 6 are used for each

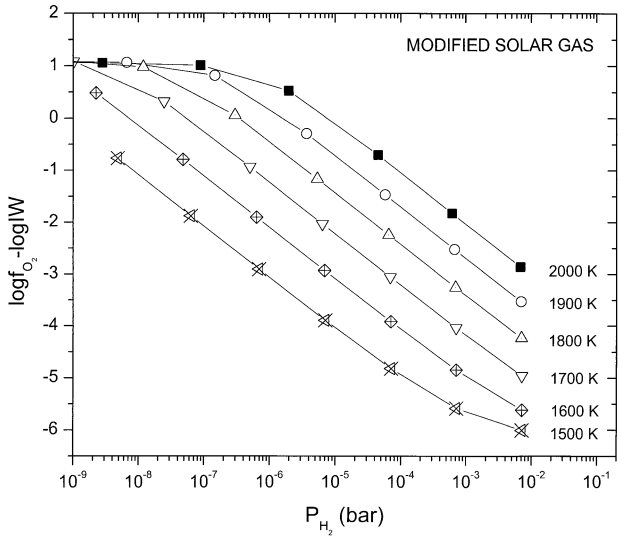

Fig. 3. The logarithm of the oxygen fugacity relative to that of the iron-wüstite buffer at the surface of a droplet of composition δ in a modified solar gas, plotted as a function of the partial pressure of H_2 for various temperatures. The oxygen fugacity at the surface of a CMAS droplet evaporating into a solar gas is almost always higher than that of the ambient gas, whose log $fO_2 \sim$ IW-6 in this temperature range.

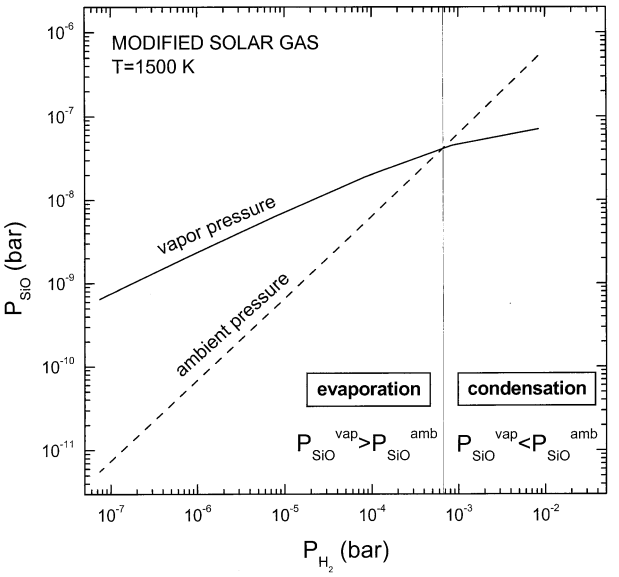

Fig. 4. At constant temperature, both the vapor pressure of $SiO_{(g)}$ over a droplet of composition δ and the ambient pressure of $SiO_{(g)}$ in a modified solar gas increase with hydrogen pressure. At 1500 K, the curves cross at $P_{H_2} = 6.7 \times 10^{-4}$ bar, causing condensation of silicon above this pressure and evaporation below it.

of the 11 elements, but all expressions of liquid-gas equilibrium like Eqn. 9 and 10 are omitted. Thus, P_i^{amb} is the partial pressure of species *i* expected in the ambient gas uninfluenced thermodynamically by the droplet, but at the same P_H^{tot} and temperature as the conditions of evaporation. P_i^{amb} is always calculated from solar relative elemental abundances modified by the fraction of each condensable element present in the droplet.

Examination of Eqn. 14 reveals that it is actually an expression for the net flux of a species across the droplet/gas interface, i.e., the difference between an outgoing, or evaporation, flux and an incoming, or condensation, flux. The numerator of Eqn. 14 is sometimes written as the difference between the product of an evaporation coefficient and P_i^{vap}, and the product of a condensation coefficient and P_i^{amb}. Throughout this paper, however, it is assumed that the evaporation and condensation coefficients are equal to one another for each species evaporating from CMAS liquids into H-rich gases, in the absence of any information to the contrary. The same variation of α_{Mg} with temperature and the same α_{SiO}/α_{Mg} ratio of 1.35 were employed as in Grossman et al. (2002). All species of the same element are assumed herein to have equal evaporation coefficients. In the absence of experimental data and because of similarities in their structural roles in silicate melts, all species of Ca were assumed to have the same α as $Mg_{(g)}$, and all species of Al the same α as $SiO_{(g)}$. The total flux of an element is obtained by summing the fluxes of all species containing that element, each one multiplied by a stoichiometric coefficient. To a very good approximation, however, the total fluxes of the elements Mg and Si are the fluxes of $Mg_{(g)}$ and $SiO_{(g)}$, respectively, over the range of conditions explored in this work. The density of the liquid was allowed to vary with temperature and composition according to the model of Lange and Carmichael (1987). As a result, the densities are generally lower by several percent in this work than in Grossman et al. (2002).

Note that, if $P_i^{vap} > P_i^{amb}$, the net flux is positive and evaporation of species *i* occurs but if $P_i^{vap} < P_i^{amb}$, the net flux is negative and condensation of *i* occurs. In Figure 4, P_{SiO}^{vap} is calculated over composition δ in modified solar gas at 1500 K and plotted along with the calculated P_{SiO}^{amb} as a function of P_{H_2}. Note that P_{SiO}^{vap} increases with P_{H_2}, as in Figure 2d. P_{SiO}^{amb} also increases with P_{H_2} in the usual way, but more steeply than does P_{SiO}^{vap}, such that a critical value of P_{H_2} is reached where they are exactly equal. Thus for each temperature, there is a critical value of P_{H_2} for each element, below which the element evaporates from a liquid of composition δ into modified solar gas, and above which it condenses. At the critical P_{H_2} for a given temperature, the concentration of that element in a liquid of composition δ is in equilibrium with the ambient modified solar gas.

3.1.2. Isotopic fluxes

Because the vapor pressure of each isotopic species of $Mg_{(g)}$ and $SiO_{(g)}$ is known, the net flux of each isotopic species can be obtained by writing the Hertz-Knudsen equation for each, treating each isotope as if it were a separate element. Thus,

$$J_{25} = \frac{\alpha_{Mg}(X_{25}P_{Mg}^{vap} - Y_{25}P_{Mg}^{amb})}{\sqrt{2\pi m_{25}RT}} \quad (15)$$

and

$$J_{24} = \frac{\alpha_{Mg}(X_{24}P_{Mg}^{vap} - Y_{24}P_{Mg}^{amb})}{\sqrt{2\pi m_{24}RT}}, \quad (16)$$

where J_{25} and m_{25} are the net flux and mass, respectively, of ^{25}Mg. X_{25} and Y_{25} are the abundances of ^{25}Mg as a fraction of the total Mg in the droplet and in the ambient gas, respectively.

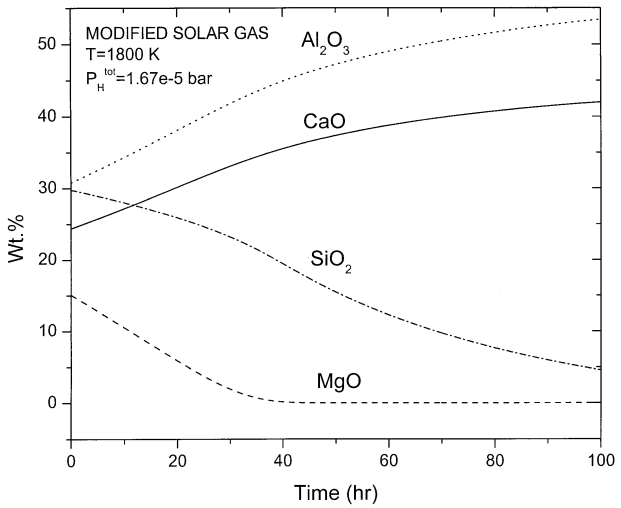

Fig. 5. Change in composition with time of a droplet of composition δ and initial radius 0.25 cm during isothermal evaporation at 1800 K into a modified solar gas with $P_{\mathrm{H}}^{\mathrm{tot}} = 1.67 \times 10^{-5}$ bar.

Like X_{25}, Y_{25} is defined such that $Y_{24} + Y_{25} + Y_{26} = 1$. Equations analogous to Eqn. 15 and 16 are also written for the net fluxes of the different isotopic species of $SiO_{(g)}$, but, for these, the vapor pressure, which appears as the first term inside the parentheses in the numerator of these equations, is expressed as in Eqn. 13. For simplicity, calculation of the masses of the different isotopic species of $SiO_{(g)}$ used in these equations assumes that all oxygen is ^{16}O. The $^{25}Mg/^{24}Mg$ ratio of the gas instantaneously traversing the droplet/gas interface is the ratio of the net fluxes of the two isotopes at any temperature, obtained by dividing Eqn. 15 by Eqn. 16,

$$\frac{J_{25}}{J_{24}} = \sqrt{\frac{m_{24}}{m_{25}}}\,\frac{(X_{25}P_{\mathrm{Mg}}^{\mathrm{vap}} - Y_{25}P_{\mathrm{Mg}}^{\mathrm{amb}})}{(X_{24}P_{\mathrm{Mg}}^{\mathrm{vap}} - Y_{24}P_{\mathrm{Mg}}^{\mathrm{amb}})}. \qquad (17)$$

3.2. Isothermal Evaporation Into an Ambient Gas

3.2.1. Computational strategy

Imagine that a parcel of gas containing equilibrium proportions of condensate nodules of composition δ and radius 0.25 cm is simultaneously compressed to a $P_{\mathrm{H}}^{\mathrm{tot}}$ of 1.67×10^{-5} bar and heated to 1800 K, whereupon they melt totally and evaporate isothermally into modified solar gas for 100 h. In the calculation whose results are shown in Figures 5 to 8, this is actually accomplished by allowing it to cool from 1800 to 1799 K at 0.01 K/h. Both the droplet and the ambient gas begin with solar isotopic composition for all elements. For illustrative purposes only, the nodule is assumed to melt completely. All of the liquid is assumed to be instantaneously in chemical communication with the vapor. At the first time step, the bulk composition and temperature are used to calculate the activities of the oxides in solution. The vapor pressure and ambient pressure of each chemical and isotopic species are then calculated and substituted into equations analogous to Eqn. 14 and 15, along with the evaporation coefficients calculated for that temperature. From the net flux of each chemical species, the total fluxes of Al and Ca are calculated in mol/cm^2-s. The total

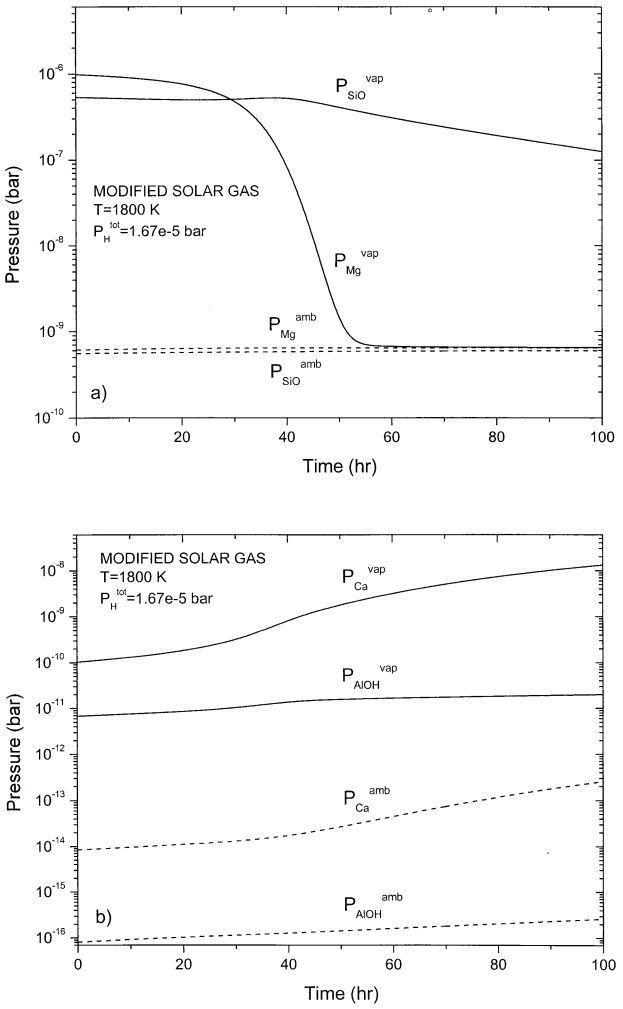

Fig. 6. Variation with time of vapor pressures, P_i^{vap}, and ambient pressures, P_i^{amb}, of the most abundant species of (a) silicon and magnesium; and (b) calcium and aluminum during isothermal evaporation at 1800 K of a droplet of composition δ and initial radius 0.25 cm into a modified solar gas with $P_{\mathrm{H}}^{\mathrm{tot}} = 1.67 \times 10^{-5}$ bar.

net flux of Mg is approximated by that of $Mg_{(g)}$ and of Si by that of $SiO_{(g)}$, and the net flux of each of these species is calculated as the sum of the net fluxes of the three isotopic species of each. From the composition and temperature of the droplet at this time step, its density and surface area are calculated. The net flux of each element and isotope is then multiplied by the surface area of the droplet and the duration of the time step to obtain the number of moles of each element and isotope evaporated in that time step. The fractional amount of each element and isotope removed from the droplet in that time step is subtracted from the amount present in the droplet. It is used to calculate the fraction of each element and isotope in the total system that was removed from the condensed fraction, and this is added to the amount that was present in the ambient gas at the beginning of the time step. The entire calculation is then repeated for the new chemical and isotopic compositions of the droplet and gas at the temperature of the next time step. In most computations, a nine-second duration was selected for each time step. As a check on the accuracy of the numerical proce-

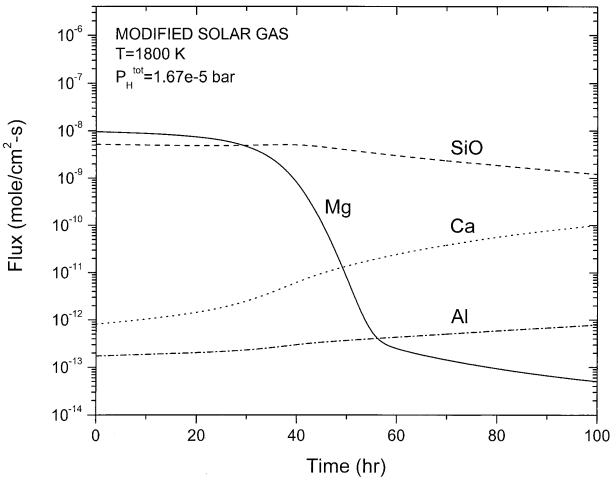

Fig. 7. Variation with time of the net fluxes of $SiO_{(g)}$ and $Mg_{(g)}$, and of the sums of the net fluxes of all species of aluminum and of calcium during isothermal evaporation at 1800 K of a droplet of composition δ and initial radius 0.25 cm into a modified solar gas with $P_H^{tot} = 1.67 \times 10^{-5}$ bar.

dure, the Mg and Si isotopic compositions of the total system were computed from the proportions and isotopic compositions of the droplet and gas components at each time step, and were always found to deviate from solar isotopic composition by no more than 10^{-2}‰ for magnesium and 10^{-3}‰ for silicon.

3.2.2. Chemical evolution

The variation in droplet composition is shown as a function of time in Figure 5. The MgO and SiO_2 contents of the droplet both fall rapidly initially. After ~40 h, however, the MgO content falls much more slowly, from ~1500 ppm to ~2.4 ppm at 100 h, while the SiO_2 content continues its relatively rapid decline, reaching 4.6 wt.%. The loss of MgO and SiO_2 enriches the droplet in CaO and Al_2O_3 whose concentrations reach 42.0 and 53.4 wt.%, respectively. The vapor pressure and ambient pressure of the dominant species of each element are shown as a function of time in Figures 6a and 6b. The vapor pressures of $Mg_{(g)}$ and $SiO_{(g)}$ decline with time, that of $Mg_{(g)}$ rather steeply, and those of $Ca_{(g)}$ and $AlOH_{(g)}$ rise, mirroring changes in the activities of their parent oxides in the liquid in response to their changing concentrations. The increases with time in the ambient pressures of $Mg_{(g)}$ and $SiO_{(g)}$ are barely perceptible, while those of $Ca_{(g)}$ and $AlOH_{(g)}$ are more marked. This reflects the fact that the preponderance of the Mg and Si is initially in the gas while that of the Ca and Al is initially in the liquid as a consequence of their distribution between δ, a typical high-temperature condensate composition, and its complementary gas. As time passes, $Mg_{(g)}$ is the only species whose vapor pressure closely approaches its ambient pressure, causing its outgoing flux to approach its incoming flux and the numerator of Eqn. 14 to approach zero. The net fluxes of the major species are shown as a function of time in Figure 7, from which it can be seen that the Mg flux becomes very small and gradually falls toward zero as the concentration of MgO in the droplet becomes vanishingly small with time. Eventually, some non-zero concentration of MgO will be reached

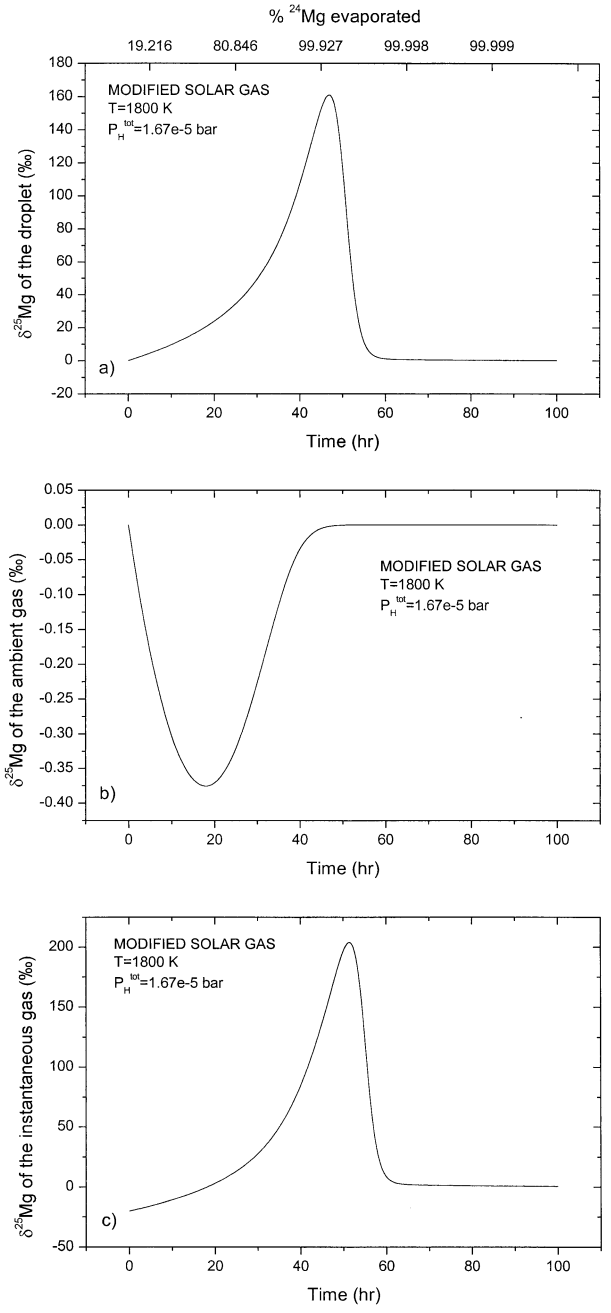

Fig. 8. Variation in δ^{25}Mg with temperature of (a) the residual droplet; (b) the ambient gas; and (c) the net gas instantaneously traversing the gas/droplet interface during isothermal evaporation at 1800 K of a droplet of composition δ and initial radius 0.25 cm into a modified solar gas with $P_H^{tot} = 1.67 \times 10^{-5}$ bar. The fraction of the initial ^{24}Mg evaporated at various evaporation times is shown along the top of (a).

which will support a vapor pressure of $Mg_{(g)}$ exactly equal to its ambient pressure, and Mg evaporation will cease, even as evaporation of Si continues. At that point, the MgO concentration of that liquid composition will be in equilibrium with the ambient pressure of $Mg_{(g)}$ at this particular temperature and P_H^{tot}.

3.2.3. Isotopic evolution

For the same evaporation conditions, δ^{25}Mg of the droplet, the ambient gas and the gas instantaneously traversing the droplet/gas interface are plotted as a function of time in Figures 8a, 8b, and 8c, respectively. In this work, it is important to note that δ^{25}Mg of the instantaneous gas is not that of the outgoing flux but rather that of the net flux, i.e., the isotopic composition of the net gas lost from or added to the droplet at each step. Both the droplet and the ambient gas start at δ^{25}Mg = δ^{26}Mg = 0. As seen in Figure 8c, the very first gas to evaporate has δ^{25}Mg = −20.23‰, as the isotopic masses used in this work yield a gas/liquid fractionation factor of $\sqrt{23.985042/24.985837}$ = 0.97977. Because δ^{25}Mg of the instantaneous gas is negative, δ^{25}Mg of the droplet increases and that of the coexisting gas decreases. As evaporation proceeds, the increase in δ^{25}Mg of the droplet is much greater than the decrease in that of the coexisting gas, as there is almost 20 times as much Mg in the gas reservoir initially as there is in the droplets. As δ^{25}Mg of the droplet increases, so does δ^{25}Mg of the instantaneous gas but the difference between them narrows. At ~17.8 h, δ^{25}Mg of the instantaneous gas becomes higher than that of the ambient gas, causing the trend of δ^{25}Mg in the ambient gas to reverse itself and increase thereafter. δ^{25}Mg of the outgoing flux must always be less than that of the droplet, and it is partially offset by an incoming flux from the ambient gas whose δ^{25}Mg is always ~0. This may allow δ^{25}Mg of the net gas crossing the interface, the instantaneous gas, to become greater than that of the droplet, particularly when the MgO concentration becomes so small that the outward flux of Mg approaches that of the incoming flux. In the present example, this occurs at ~47 h, when >99.97% of the ^{24}Mg has evaporated and there is only ~36 ppm Mg remaining in the droplet. Here, the droplet and the instantaneous gas have the same δ^{25}Mg, ~+161‰, and, after this time, the instantaneous gas has a higher δ^{25}Mg than the droplet. This causes the trend of δ^{25}Mg in the droplet to reverse itself, with the droplet decreasing its δ^{25}Mg as evaporation continues. In the final time step, with the concentration of MgO still falling very slowly toward some very small equilibrium value, δ^{25}Mg of the ambient gas and droplet are -10^{-7} and +0.167‰, respectively, and the difference between them is also narrowing very slowly with time. In isothermal runs of the same temperature and duration but at higher P_H^{tot}, the difference in δ^{25}Mg between the droplet and ambient gas is $<10^{-3}$‰ in the final time step because both the evaporation rate and the incoming flux of $Mg_{(g)}$ are higher.

δ^{29}Si of the droplet, the ambient gas and the gas instantaneously traversing the droplet/gas interface are plotted as a function of time in Figures 9a, 9b, and 9c, respectively. Both the droplet and coexisting gas start at δ^{30}Si = δ^{29}Si = 0. The Si isotopic evolution behaves in almost exactly the same way as Mg, with two exceptions. First, unlike Mg, an equilibrium fractionation factor is assumed which yields a Si isotopic vapor pressure ratio different from the Si isotopic activity ratio. As a result, the overall gas/liquid partition coefficient for the ^{29}Si/^{28}Si ratio can be thought of as the product of that equilibrium fractionation factor, and a kinetic fractionation factor which causes ^{28}Si to be removed more quickly than ^{29}Si, even at equal vapor pressures. Thus, as seen in Figure 9c, the first vapor removed from the droplet at 1800 K has δ^{29}Si = −11.87‰,

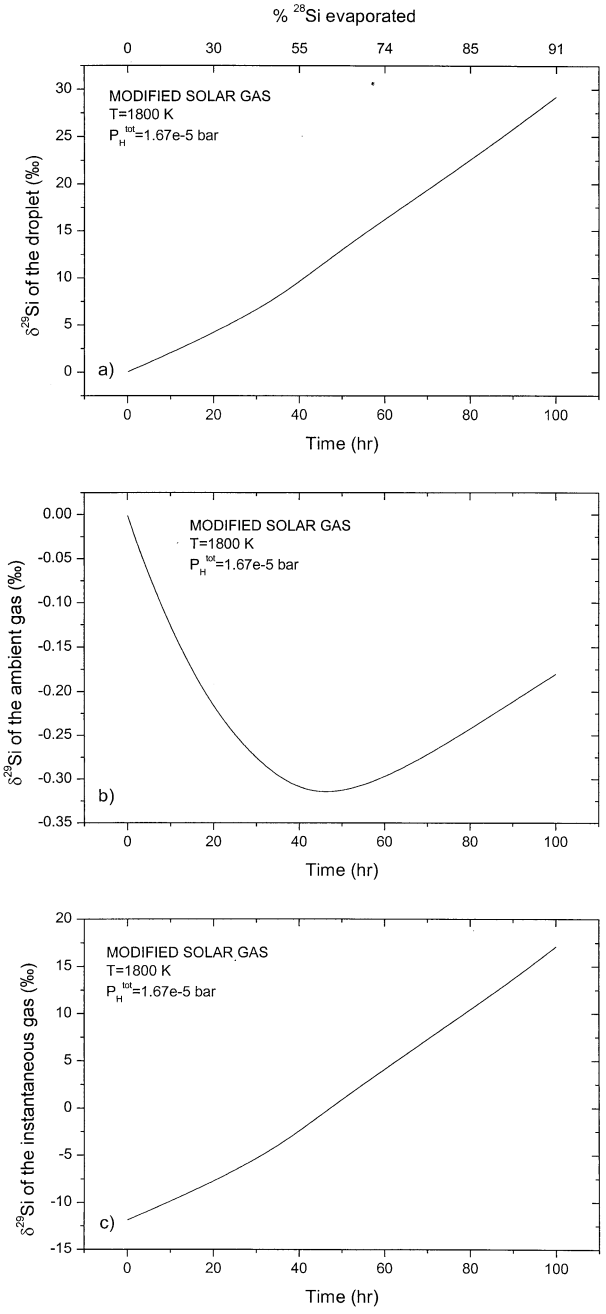

Fig. 9. Variation in δ^{29}Si with temperature of (a) the residual droplet; (b) the ambient gas; and (c) the net gas instantaneously traversing the gas/droplet interface during isothermal evaporation at 1800 K of a droplet of composition δ and initial radius 0.25 cm into a modified solar gas with P_H^{tot} = 1.67 × 10^{-5} bar. The fraction of the initial ^{28}Si evaporated at various evaporation times is shown along the top of (a).

due to an equilibrium $(^{29}Si/^{28}Si)_{gas}/(^{29}Si/^{28}Si)_{liquid}$ = 0.99929 and a kinetic fractionation factor of $\sqrt{43.976327/44.975894}$ = 0.98883. Second, since much less Si evaporates than Mg and because the overall gas/liquid fractionation factor is smaller for the ^{29}Si/^{28}Si than for the ^{25}Mg/^{24}Mg ratio, variations in δ^{29}Si of the droplet, Figure 9a, are much less than those of δ^{25}Mg, Figure 8a, under the same conditions. After 100 h of evapora-

tion, δ^{29}Si of the instantaneous gas has overtaken that of the ambient gas but has not yet overtaken that of the droplet. The ambient gas reaches a minimum δ^{29}Si of -0.31‰ and a final value of -0.18‰, and δ^{29}Si of the droplet reaches 29.2‰. In isothermal runs at the same temperature but for 10^4 h at higher ambient pressure, both evaporation of Si and Si isotopic equilibration of the droplet with the ambient gas are more complete. In the final time step of such runs, the difference in δ^{29}Si between the droplet and ambient gas is 0.70‰, just as expected from the equilibrium fractionation factor at 1800 K adopted in this work.

The phenomenon of rising and then declining heavy isotope enrichment of a residue during progressive evaporation was also predicted in theoretical studies of closed-system evaporation of forsterite into a Mg-containing ambient gas (Tsuchiyama et al., 1999) and of isothermal evaporation of general binary mixtures into an ambient gas containing the same elements (Ozawa and Nagahara, 2001). That the heavy isotope enrichment of the instantaneous gas can be greater than that of the residue from which it is escaping and that the residue can become less heavy-isotope-enriched with progressive evaporation are a consequence of the form of Eqn. 17. In this equation, the ^{25}Mg/^{24}Mg ratio of the instantaneous gas is merely the ratio of net fluxes, J_{25}/J_{24}. Recall that the net flux of each isotope depends on the difference between its outgoing and incoming flux. This, in turn, depends on the difference in the abundance of the isotope as a fraction of the total Mg between the droplet and the ambient gas. Because ^{24}Mg evaporates more readily than ^{25}Mg, the isotopic proportion of ^{24}Mg initially falls more rapidly in the droplet and rises more rapidly in the ambient gas than in the case of ^{25}Mg. As a result, the net flux of ^{24}Mg and the denominator of Eqn. 17 decrease faster than the net flux of ^{25}Mg and the numerator, causing the ^{25}Mg/^{24}Mg ratio of the instantaneous gas to become very large. Another way of viewing this is that domination of the incoming flux over the outgoing flux begins sooner for ^{24}Mg than for ^{25}Mg. This phenomenon is referred to as "isotope exchange" or "back-reaction" between the residue and the ambient gas. The term isotope exchange usually refers to a process in which the elemental concentrations remain constant in the phases exchanging with one another, and the term back-reaction implies net addition of the element from the ambient gas into the residue. In the calculations presented here, however, it is important to note that reduction in δ^{25}Mg of the droplet occurs while the net flux of each Mg isotope is still positive and the concentration of each Mg isotope in the droplet is still declining, i.e., while net evaporation of Mg continues.

The effect seen in these calculations is probably the one observed by Craig et al. (1963) during experiments on evaporation of water into air of nonzero humidity. In these, the δ^{18}O of residual water rose and then leveled off with increasing degree of evaporation beyond ~85%. This could happen only if the net vapor lost from the late residues had the same δ^{18}O as the latter. Similarly, Lloyd (1966) observed natural hypersaline waters whose δ^{18}O rose, leveled off and then fell with increasing salinity. This could happen only if the δ^{18}O of the net water lost from the most evaporated samples exceeded that of the residual water.

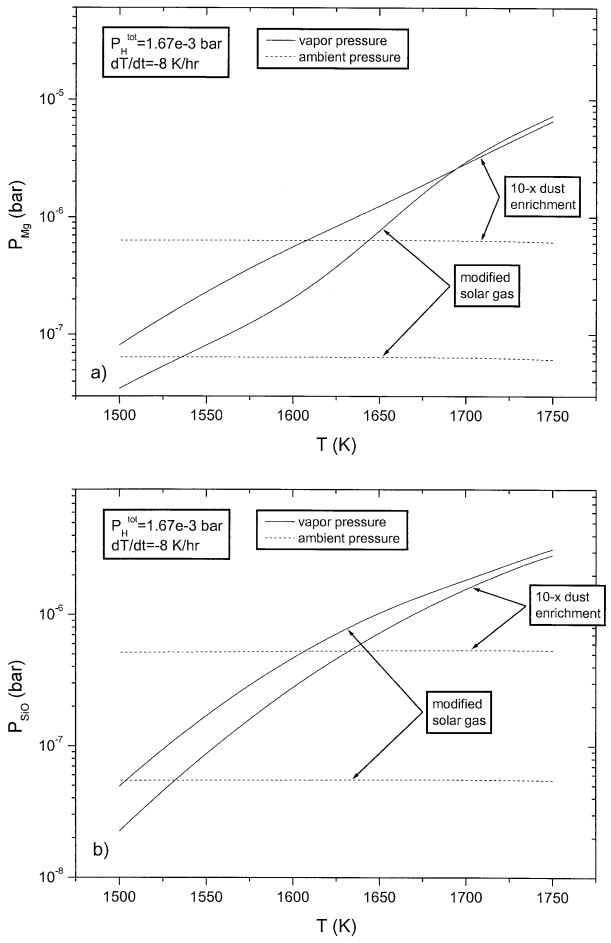

Fig. 10. Variation with temperature of the vapor pressure and ambient pressure of (a) $Mg_{(g)}$; and (b) $SiO_{(g)}$ during evaporation of a droplet of composition δ and initial radius 0.25 cm while cooling from 1750 to 1500 K at 8 K/h. Two cases are compared, one in which evaporation occurs in a modified solar gas and the other in a system enriched in C1 dust relative to solar composition by a factor of 10, both at $P_H^{tot} = 1.67 \times 10^{-3}$ bar.

3.3. Evaporation Into an Ambient Gas During Cooling

3.3.1. Modified solar gas

Now suppose that a parcel of gas containing equilibrium proportions of condensate nodules of composition δ and radius 0.25 cm is instantaneously compressed to a P_H^{tot} of 1.67×10^{-3} bar and heated to 1750 K. Suppose further that the nodules melt totally, remain completely molten and evaporate into modified solar gas of constant P_H^{tot} during cooling at 8 K/h until the solidus temperature, 1500 K, is reached, where the calculation ceases. The temperature variation of the vapor pressures of $Mg_{(g)}$ and $SiO_{(g)}$ are shown in Figures 10a and 10b, respectively, where they are compared with their ambient pressures. The vapor pressures of both species decline with falling temperature while their ambient pressures again increase almost imperceptibly. In this case, the vapor pressures of both $Mg_{(g)}$ and $SiO_{(g)}$ decline sufficiently that they not only reach their respective ambient pressures but also fall below them, $Mg_{(g)}$ at 1536 K and $SiO_{(g)}$ at 1504 K, causing their net fluxes to

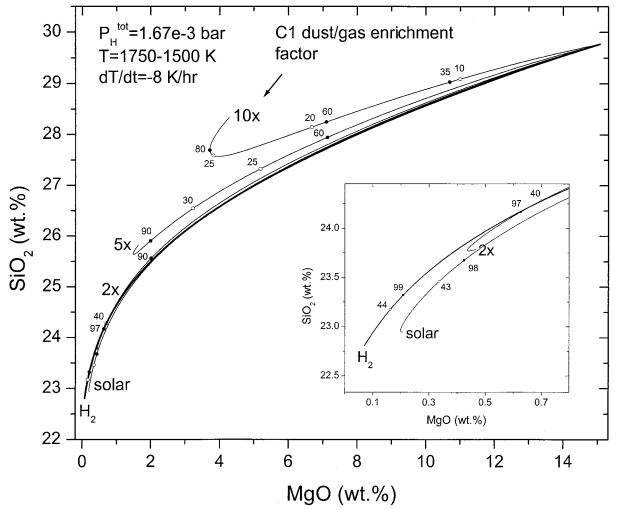

Fig. 11. Evolution of the composition of a droplet of composition δ and initial radius 0.25 cm during evaporation while cooling from 1750 to 1500 K at 8 K/h. Different paths are shown for evaporation into pure H_2, into modified solar gas, and in systems enriched in C1 dust relative to solar composition by factors of 2, 5 and 10, each at $P_H^{tot} = 1.67 \times 10^{-3}$ bar. Along each curve, numbers at open and closed circles give % ^{28}Si and % ^{24}Mg evaporated, respectively.

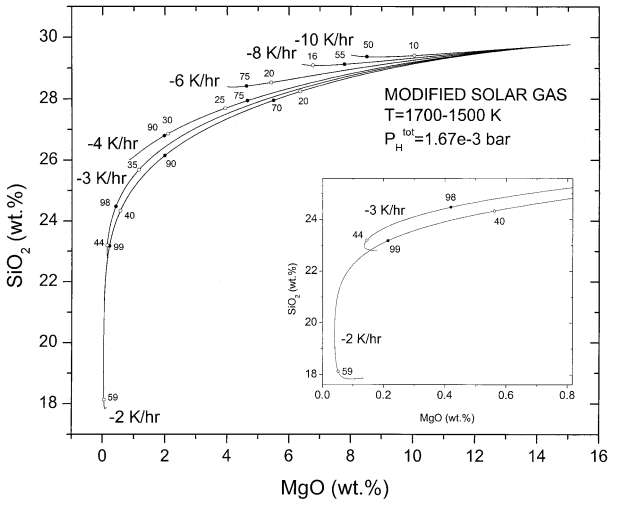

Fig. 12. Evolution of the composition of a droplet of composition δ and initial radius 0.25 cm during evaporation into modified solar gas at $P_H^{tot} = 1.67 \times 10^{-3}$ bar while cooling from 1700 to 1500 K at various rates. Data points labeled as in Figure 11.

become negative at these temperatures. This behavior is thus significantly different from the isothermal case, in which the vapor pressure never falls below the ambient pressure and the net flux never becomes negative. The difference is that, in the present case, the variable temperature provides an additional degree of freedom that is absent in the isothermal case.

The evaporation-induced declines in the concentrations of MgO and SiO_2 in the liquid are shown in Figure 11. In the inset, note that there is a very slight increase in MgO content at the low-MgO end of the modified solar gas curve. This is due to the fact that the $Mg_{(g)}$ flux became negative, and MgO began to condense. The reason why this produced such a small increase in MgO content is that the flux became negative at 1536 K. Because the evaporation coefficients fall with decreasing temperature and this temperature is only 36 K above the solidus, where the calculation ends, there is little opportunity for significant condensation into the liquid. An analogous uptick in the SiO_2 content, due to the flux of $SiO_{(g)}$ becoming negative only 4 K before the end of the calculation, is overwhelmed by the opposite effect of dilution by MgO addition.

3.3.2. *Cooling rate effects*

A series of calculations was performed to monitor the change in chemical and isotopic composition of δ accompanying evaporation into modified solar gas at $P_H^{tot} = 1.67 \times 10^{-3}$ bar during cooling from 1700 to 1500 K over a range of cooling rates from 2 to 10 K/h. This is within the range of cooling rates estimated for refractory inclusions on the basis of melilite zoning produced in dynamic crystallization experiments (MacPherson et al., 1984) and from previous estimates of evaporative losses of Mg and Si (Grossman et al., 2002). The change in bulk chemical composition of δ is shown in Figure 12. The main effect of cooling rate is to change the total time duration of the evaporation process, from 20 h at 10 K/h to 100 h at 2 K/h. Because MgO is more volatile than SiO_2 under these conditions, the reduction in MgO content of the droplet is much greater than that of SiO_2 at every cooling rate. Between 10 and 4 K/h, the rate of decline of the MgO content is so much greater than that of SiO_2 that the SiO_2 content actually increases slightly at the low-MgO, i.e., low-temperature, ends of the curves. At each of these cooling rates, although the vapor pressures of $Mg_{(g)}$ and $SiO_{(g)}$ decline with the concentrations of their parent oxides, neither becomes as low as its ambient pressure and thus neither element condenses. At lower cooling rates, however, where more evaporation occurs, the vapor pressures of both species fall below their ambient pressures, causing condensation of MgO and SiO_2 at 1558 and 1504 K, respectively, at 3 K/h, and 1623 and 1535 K, respectively, at 2 K/h, and producing reversals at the ends of the curves for these cooling rates (Fig. 12, inset).

3.3.3. *Comparison with previous work*

Evaporation calculations in 10^{-6} bars of pure $H_{2(g)}$ were used successfully by Grossman et al. (2002) to explain the bulk chemical compositions of refractory inclusions. In that work, a suite of appropriate condensate starting compositions was assumed, a maximum temperature was assigned to each on the basis of petrologic criteria, and the chemical and isotopic evolution of a liquid droplet of each composition was computed during simultaneous crystallization and evaporation over a range of cooling rates from 0.07 to 12 K/h. The present study investigates, in the absence of crystallization, the effect of substituting a modified solar gas for pure $H_{2(g)}$ on the chemical and isotopic evolution during evaporation of a liquid droplet of composition δ, only one of the compositions studied in the earlier work.

In Figure 11, just such a chemical evolution path is compared to one labelled "H_2." The latter curve is that which would have been calculated by Grossman et al. (2002) for evaporation into

pure $H_{2(g)}$ over the same temperature range and at the same P_H^{tot} and cooling rate as in the modified solar gas case had simultaneous crystallization of the liquid been suppressed. If the gas composition were the only difference between the two calculations, the fO_2 would have been slightly higher at each temperature step in the case of evaporation into modified solar gas than into pure $H_{2(g)}$, causing the vapor pressures of both $Mg_{(g)}$ and $SiO_{(g)}$ to be slightly lower in the modified solar gas case. This, together with the fact that the ambient pressures of both $Mg_{(g)}$ and $SiO_{(g)}$ are nonzero in modified solar gas, would have caused the net fluxes of both species to be lower at each temperature step in this case. Thus, the total amounts of MgO and SiO_2 evaporated by the time the temperature falls to 1500 K would have been slightly less in the case of modified solar gas, causing their final concentrations in the droplet to be slightly higher than in the case of pure $H_{2(g)}$. There are, however, two other differences in the treatment of liquid evaporation between the work of Grossman et al. (2002) and the present study, both of which tend to increase the evaporation rate in the present work, thus counteracting the effect of the difference in gas composition. The first is the previously mentioned, more accurate treatment of liquid density in the present study. This leads to fewer atoms in a droplet of a given size but leaves activities and thus absolute evaporation rates unchanged, resulting in higher fractional evaporation rates. The second lies in the way hydrogen is treated in the two studies. In Grossman et al. (2002), P_{H_2} was held constant despite the fact that $H_{2(g)}$ is consumed in reactions with MgO and SiO_2 in the droplet to form $H_2O_{(g)}$. A more realistic approach, to hold P_H^{tot} constant, is adopted in the present study. Because the equilibrium constants of $H_{2(g)}$-consuming reactions such as Eqn. 9 decrease with falling temperature, P_{H_2O} also decreases with falling temperature. Thus, when a value of P_H^{tot} is selected to yield the same P_{H_2} at a particular initial temperature in this work as one used in Grossman et al. (2002), the P_{H_2}/P_{H_2O} ratio increases more with falling temperature in the present work, causing slightly more evaporation in this study. As a result of all these effects, Figure 11 shows that the final concentrations of MgO and SiO_2 are only very slightly higher, 0.21 and 22.94%, respectively, in the modified solar gas case than in pure $H_{2(g)}$, 0.07 and 22.81%, at the stated physical conditions. Because the differences between vapor pressures and ambient pressures of $Mg_{(g)}$ and $SiO_{(g)}$ decrease with increasing P_H^{tot} (Fig. 4), the difference in final MgO and SiO_2 contents between the modified solar gas case and the pure $H_{2(g)}$ case increases with increasing P_H^{tot}. The difference in final MgO and SiO_2 contents between the modified solar gas case and the pure $H_{2(g)}$ case also increases with decreasing cooling rate. For example, for evaporation over the same temperature range and at the same P_H^{tot} as in Figure 11 but at a cooling rate of 5 K/h, the final MgO and SiO_2 contents are 0.0 and 15.09%, respectively, in pure $H_{2(g)}$ but 0.09 and 16.59% in modified solar gas.

It has thus been shown that applying the methods of Grossman et al. (2002) to evaporation of completely molten droplets in pure $H_{2(g)}$ leads to very similar chemical evolution paths as in modified solar gas, with the differences becoming larger with increasing ambient pressure and decreasing cooling rate. Even at a P_H^{tot} as high as 1.67×10^{-3} bar and a cooling rate as low as 5 K/h, evaporation paths are almost identical in the two treatments, except at the low-temperature, low-MgO ends of the curves where the degree of evaporation is most extreme. As Grossman et al. (2002) did not require extreme degrees of evaporation to explain the chemical compositions of refractory inclusions, their conclusions are equally valid in modified solar gas. The remainder of this paper focusses on the behavior of this system at greater evaporative losses of Mg and Si than investigated in that work, particularly at enhanced dust/gas ratios and/or relatively high P_H^{tot}, where the effects of ambient pressure are greater than those seen above.

3.3.4. Dust-enriched systems

The effects of the reversal of the evaporation process into a condensation process during cooling of the droplet are accentuated in dust-enriched gases. To see this, the modified solar gas calculation whose results are shown in Figure 11 was repeated under the same conditions and in an identical way except that the elemental abundances in the total system were changed to those computed by Ebel and Grossman (2000) for systems enriched in dust of C1 composition relative to the gas. If the condensable fraction of an interstellar cloud of solar composition overall is present as dust of C1 composition, and the dust concentrates in certain regions relative to the gas before gravitational collapse of the cloud, heating and total evaporation of the dust, then the Ebel and Grossman (2000) compositions apply to those regions. The variation with temperature of the composition of the equilibrium condensate assemblage generally differs at different degrees of dust enrichment. Although high-temperature condensate nodules with the exact composition of δ would not be predicted to form under these conditions, those that do form will have compositions generally similar to δ. Nevertheless, for purposes of comparison only, it was assumed in the calculations whose results follow that the initial composition of the droplet and the initial distribution of elements between condensate and gas are exactly as given above for δ.

The vapor pressures and ambient pressures in a system with a C1 dust/gas enrichment factor of 10 are compared with those in a system of solar composition for $Mg_{(g)}$ and $SiO_{(g)}$ in Figures 10a and 10b, respectively. As the ratio of the abundance of each condensable element to that of H increases by the same factor as the dust/gas enrichment, the ambient pressure of each increases by a factor of 10 in the dust-enriched case in accordance with Eqn. 4. This level of dust enrichment reduces the net fluxes of both $SiO_{(g)}$ and $Mg_{(g)}$ compared to the modified solar gas case. As a result, both the SiO_2 and MgO contents of the droplet fall by lesser amounts in the dust-enriched case than in the modified solar gas case, leading to higher SiO_2 and MgO contents at each temperature step in the dust-enriched case. Since the MgO contents are so much lower than the SiO_2 contents in the modified solar gas case, however, the small absolute concentration increases in dust-enriched gas produce much greater relative concentration increases, and thus much greater relative activity increases, in MgO than in SiO_2. As can be seen from the first term in Eqn. 8, the vapor pressure of $Mg_{(g)}$ depends upon the product of the activity of MgO in the liquid and the P_{H_2}/P_{H_2O} ratio at the droplet surface. The vapor pressure of $SiO_{(g)}$ is related to the SiO_2 activity through an otherwise identical expression. The enhanced fO_2 of the dust-enriched gas produces a P_{H_2}/P_{H_2O} ratio at the droplet surface

which is ~10% lower than that produced by modified solar gas at 1750 K, an effect which, by itself, would reduce the vapor pressures of both $Mg_{(g)}$ and $SiO_{(g)}$ by the same amount compared to the modified solar gas case. For Si, the vapor pressure reduction due to the fO_2 effect of dust enrichment is greater than the vapor pressure increase due to the higher activity effect of dust enrichment, but for Mg the opposite is true. Consequently, the vapor pressure of $SiO_{(g)}$ is always less in the dust-enriched case than in the modified solar gas case in Figure 10b but the vapor pressure of $Mg_{(g)}$, which is lower in the dust-enriched case at high temperature in Figure 10a, becomes larger in dust-enriched gas than in modified solar gas as the temperature falls. The important point, however, is that the vapor pressure drops below the ambient pressure for both $Mg_{(g)}$ and $SiO_{(g)}$, causing initiation of condensation of both MgO and SiO_2, at much higher temperatures, 1608 and 1632 K, respectively, in the dust-enriched case than in modified solar gas. The effect of all this on the evolution of the bulk chemical composition of the evaporating droplet is shown in Figure 11, where the evolutionary track at 10× dust enrichment is compared with the cases for 5× and 2× dust enrichment, as well as with the solar gas case. The higher the dust enrichment, the more retarded is the evaporation of both Mg and Si before condensation, the higher is the temperature of the beginning of condensation of each, and the higher are the minimum and final concentrations of both MgO and SiO_2 reached during cooling to 1500 K.

3.3.5. *Magnesium isotopic fractionations*

It is instructive to explore the Mg isotopic evolution of the system during cooling at 2 K/h. δ^{25}Mg of the droplet, the ambient gas and the gas instantaneously traversing the droplet/gas interface are plotted as a function of temperature in Figures 13a, 13b, and 13c, respectively. The curves in these figures are very similar to those seen for isothermal evaporation, Figures 8a, 8b, and 8c, respectively, with δ^{25}Mg of the instantaneous gas overtaking that of the ambient gas at ~1685 K and that of the droplet at ~1654 K, where >98.99% of the ^{24}Mg has evaporated and there is only ~1304 ppm Mg remaining in the droplet. At ~1623 K, however, Figure 13c shows that δ^{25}Mg of the gas instantaneously traversing the droplet/gas interface rises steeply to $+\infty$, reappears at $-\infty$ and then rises steeply toward zero. This behavior is a consequence of the different rates at which the net fluxes of the different isotopes decrease and consequently the different temperatures at which the net flux of each isotope passes through zero. In Figure 14, J_{24} is seen to be falling much more steeply than J_{25} with declining temperature for the same reasons outlined above for isothermal evaporation. As a result, J_{24} becomes zero at a temperature which is a fraction of a degree higher than that where J_{25} becomes zero. When J_{24} becomes zero, the denominator of Eqn. 17 becomes zero, and δ^{25}Mg of the instantaneous gas becomes $+\infty$. At a slightly lower temperature, J_{24} becomes a very small negative number and J_{25}/J_{24} becomes a very large negative number as net condensation of ^{24}Mg begins while net evaporation of ^{25}Mg is still occurring. As the temperature falls, J_{24} becomes a larger negative number and J_{25} is still positive, so J_{25}/J_{24} becomes less negative, eventually becoming zero when J_{25} reaches zero. Below this temperature, net condensation of both ^{25}Mg and ^{24}Mg occur but, as seen in Figure 14, the condensation rate of ^{24}Mg is much greater than that of ^{25}Mg, yielding a negative δ^{25}Mg for the condensing gas. This eventually causes δ^{25}Mg of the droplet to become negative with very little effect on δ^{25}Mg of the ambient gas, as virtually all Mg is in the vapor phase at this stage, and the concentration of MgO in the droplet is very

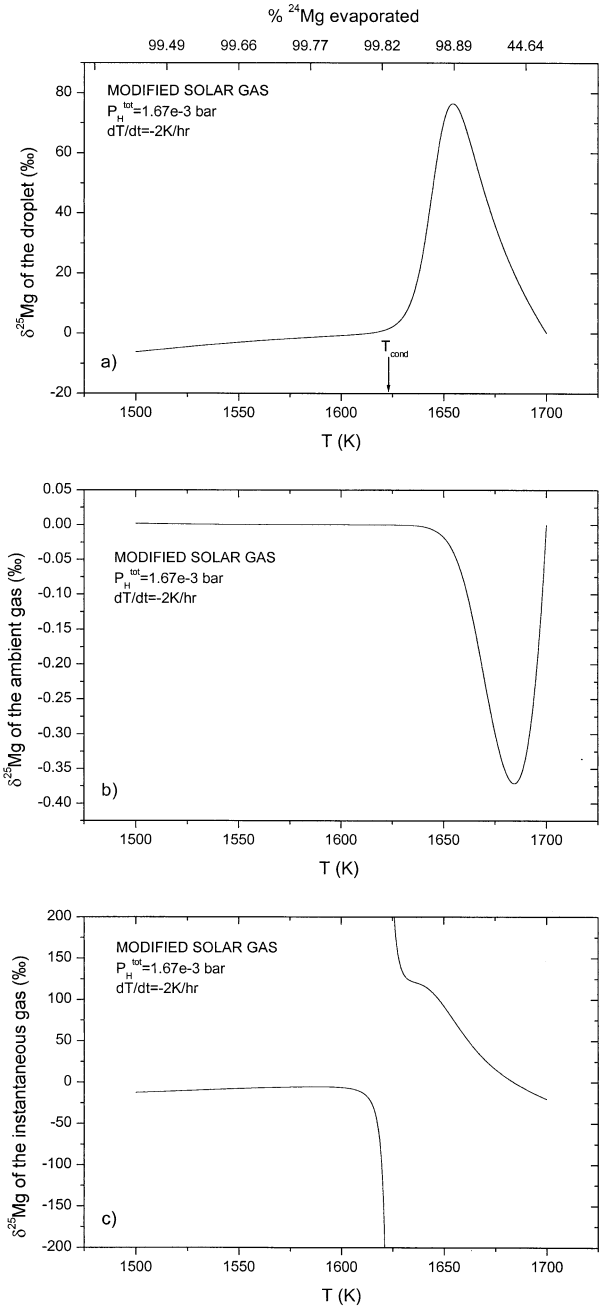

Fig. 13. Variation in δ^{25}Mg with temperature of (a) the residual droplet; (b) the ambient gas; and (c) the net gas instantaneously traversing the gas/droplet interface during evaporation of a droplet of composition δ and initial radius 0.25 cm into a modified solar gas at $P_H^{tot} = 1.67 \times 10^{-3}$ bar while cooling from 1700 to 1500 K at 2 K/h. The fraction of the initial ^{24}Mg evaporated at various temperatures is shown along the top of (a).

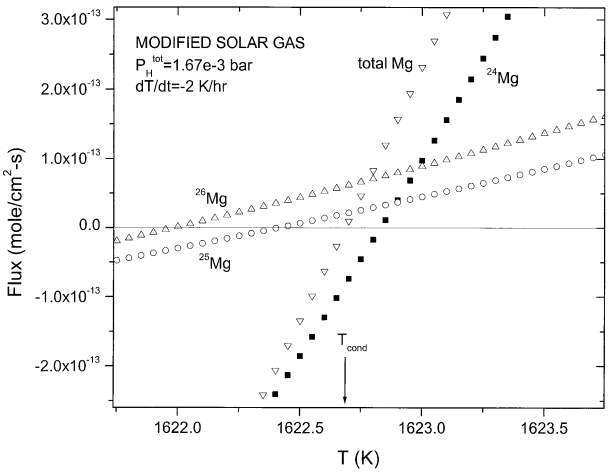

Fig. 14. Variation with temperature of the net flux of ^{24}Mg, ^{25}Mg, ^{26}Mg and total Mg across the droplet/gas interface for a droplet of composition δ and initial radius 0.25 cm in a modified solar gas at $P_H^{tot} = 1.67 \times 10^{-3}$ bar while cooling from 1700 to 1500 K at 2 K/h. Adjacent data points are separated by 10 time steps. The flux changes sign at a slightly different temperature for each isotope. The condensation temperature is the temperature at which the net flux of total Mg first becomes negative.

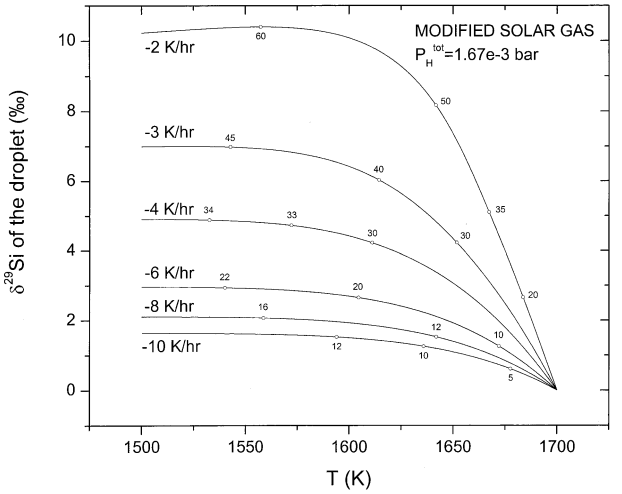

Fig. 16. Variation with temperature of δ^{29}Si of a droplet of composition δ and initial radius 0.25 cm during evaporation into a modified solar gas at $P_H^{tot} = 1.67 \times 10^{-3}$ bar while cooling from 1700 to 1500 K at various cooling rates. Data points along the curves give the fraction of initial ^{28}Si evaporated at various temperatures.

low. In this illustration, the condensation temperature of Mg, i.e., the temperature where net addition of Mg to the droplet begins, is defined by the temperature at which J_{Mg}, the sum of the net fluxes of the three isotopes, becomes zero. As seen in Figure 14, this occurs at a temperature between those where net addition of ^{25}Mg and ^{24}Mg begin to occur.

In Figure 15, the variation of the Mg isotopic composition of the droplet with temperature is illustrated for each of the cooling rates whose chemical composition changes are seen in

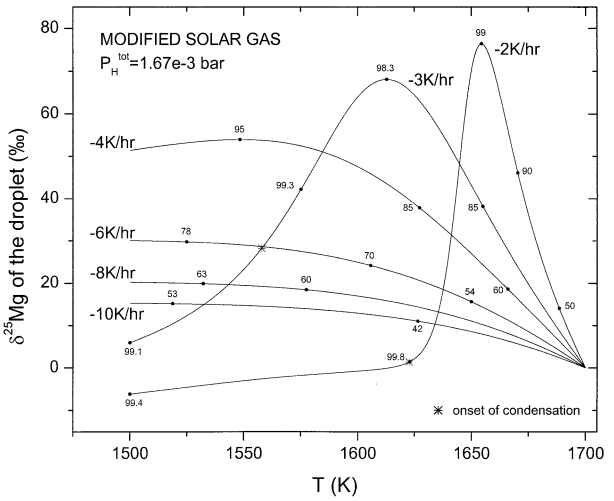

Fig. 15. Variation with temperature of δ^{25}Mg of a droplet of composition δ and initial radius 0.25 cm during evaporation into a modified solar gas at $P_H^{tot} = 1.67 \times 10^{-3}$ bar while cooling from 1700 to 1500 K at various cooling rates. Data points along the curves give the fraction of initial ^{24}Mg evaporated at various temperatures. Condensation occurs in the course of cooling at 2 and 3 K/h, and the temperatures at which this begins are marked on the curves for those cooling rates.

Figure 12. For those cooling rates at which Mg condensation occurs, 2 and 3 K/h, a higher cooling rate leads to a lower maximum δ^{25}Mg and higher final δ^{25}Mg at 1500 K. For the other cooling rates, maximum and final δ^{25}Mg both decrease with increasing cooling rate. Even though Mg condensation does not occur at 4 K/h, note that δ^{25}Mg still declines after reaching a maximum. This is due to the previously discussed tendency for reduction in the net loss rate of ^{24}Mg relative to ^{25}Mg at an extreme degree of evaporation. For all cooling rates at which δ^{25}Mg reaches a maximum, a residue can exhibit the same δ^{25}Mg at two distinctly different degrees of evaporation of Mg, distinguishable for a given starting composition only by the lower MgO concentration at the higher degree of evaporation. For example, two droplets cooled at 2 K/h, one quenched after removal from chemical communication with the vapor at 1691 K and the other at 1634 K, will both have δ^{25}Mg = 10‰, even though both temperatures are above the condensation temperature of Mg. The high-temperature one will contain 10.13 wt.% MgO after evaporation of 39% of the ^{24}Mg, and the other will contain only 0.042 wt.% after 99.8% loss of ^{24}Mg.

3.3.6. Silicon isotopic fractionations

As seen in the isothermal case, because a much smaller fraction of silicon than magnesium evaporates under these conditions and because the overall gas/liquid fractionation factor is smaller for the ^{29}Si/^{28}Si ratio than for the ^{25}Mg/^{24}Mg ratio, variations in δ^{29}Si of the droplet, shown in Figure 16, are much less than those of δ^{25}Mg. Thus, unlike the profiles of δ^{25}Mg vs. temperature at low cooling rates, those of δ^{29}Si are much flatter for a given cooling rate. Even at 2 K/h, the δ^{29}Si profile does not exhibit the sharp maximum seen for that of δ^{25}Mg, although sufficient Si is lost that the net loss rate of ^{28}Si is reduced relative to that of ^{29}Si, causing δ^{29}Si of the droplet to fall slightly at temperatures below 1557 K where >59% of the ^{28}Si is evaporated.

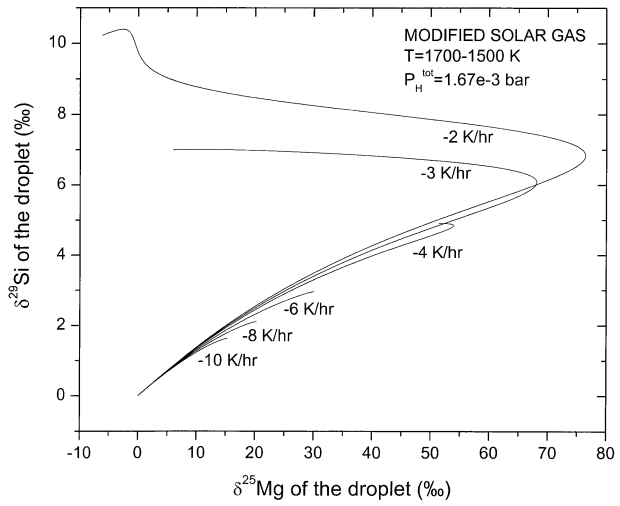

Fig. 17. Covariation of δ^{29}Si and δ^{25}Mg of a droplet of composition δ and initial radius 0.25 cm during evaporation into a modified solar gas at $P_H^{tot} = 1.67 \times 10^{-3}$ bar while cooling from 1700 to 1500 K at various cooling rates.

In Figure 17, the Si isotopic evolution of the droplet is plotted against that of Mg for each of the investigated cooling rates. While there are some cooling rates where δ^{25}Mg of the droplet first increases and then decreases as the temperature falls, δ^{29}Si constantly increases with decreasing temperature over almost the entire investigated range of cooling rates. Thus, δ^{29}Si can be used to distinguish between two droplets of the same initial composition and that have the same evaporation-induced δ^{25}Mg despite much more Mg having evaporated from one than the other at the same cooling rate. In the above example, two droplets form at 2 K/h with δ^{25}Mg = 10‰, despite the fact that one droplet loses 39% and the other >99% of its Mg. For the former, 11% of the Si evaporates, yielding δ^{29}Si of 1.4‰, while the latter loses 53% of its Si and has δ^{29}Si of 8.8‰.

As pointed out above, these two droplets can be distinguished on the basis of their vastly different MgO contents, and the SiO_2 contents are also quite different for the heavily and lightly evaporated one, 20.38 and 29.16%, respectively. The lightly evaporated one has the chemical composition of a Type B refractory inclusion but the very low MgO content of the heavily evaporated one is unlike that of any known refractory inclusion. In meteorite studies, however, it would be more common for bulk chemical compositions, δ^{25}Mg and δ^{29}Si to be known for each of a group of inclusions for which the initial bulk chemical compositions are completely unknown. If a very MgO- and SiO_2-rich starting assemblage were heavily evaporated, the refractory residue could have the same bulk chemical composition as another which formed as a result of relatively light evaporation of a less MgO- and SiO_2-rich starting material. If the heavily evaporated one, in particular, underwent evaporation under conditions of significant back-reaction of ^{24}Mg and ^{28}Si relative to the heavier isotopes of these elements, i.e., at relatively high ambient pressure, enhanced dust/gas ratio and low cooling rate, it may be possible for the final product to have very similar δ^{25}Mg and δ^{29}Si as the lightly evaporated one, in addition to similar bulk chemical composition. The different histories of these two otherwise very similar objects might be preserved in the isotopic zoning of their constituent minerals. Grossman et al. (2002) suggested that melilite in Types A and B refractory inclusions may have preserved the changing isotopic composition of the liquid from which it crystallized in the form of a series of isotopically distinct growth layers within each crystal, which may not have been homogenized either during or after the crystals grew. Thus, in the case of the heavily evaporated refractory residue envisioned here, crystals of one or more of the constituent minerals may record a progressive increase followed by a progressive decrease in δ^{25}Mg and δ^{29}Si while, in the lightly evaporated one, crystal zoning may record only monotonic increases in these ratios.

3.3.7. *Non-Rayleigh isotope fractionation by evaporation into ambient gas*

Tsuchiyama et al. (1999), Humayun and Cassen (2000) and Ozawa and Nagahara (2001) showed that the relationship between the degree of heavy isotope enrichment in an evaporation residue and the fraction of the element evaporated into a gas having nonzero pressure of the element does not follow the Rayleigh fractionation law for evaporation in vacuum. They showed further that the degree of departure from Rayleigh fractionation increases as the ratio of the ambient pressure of the evaporating element to its vapor pressure increases. As seen in Figure 4, this ratio increases as P_{H_2} increases at constant temperature. In the present calculations, P_{H_2} increases with P_H^{tot}, and at any given P_H^{tot}, temperature is a variable. As the temperature falls, the vapor pressure falls and the ambient pressure increases because the evaporating element is gradually transferred from the droplet to the ambient gas. Nevertheless, at any given temperature step, the $P_{Mg}^{amb}/P_{Mg}^{vap}$ ratio increases with P_H^{tot}.

Thus, to investigate non-Rayleigh isotope fractionation, a series of calculations was performed in which the chemical and isotopic evolution of composition δ were monitored while it evaporated into modified solar gas over a range of P_H^{tot} from 1.67×10^{-4} to 1.67×10^{-2} bar during cooling from 1700 to 1500 K at 4 K/h. The $P_{Mg}^{amb}/P_{Mg}^{vap}$ ratio increases from the beginning to the end of each calculation, from 4.0×10^{-3} to 4.3×10^{-2} at $P_H^{tot} = 1.67 \times 10^{-4}$ bar, 1.3×10^{-2} to 0.7 at 1.67×10^{-3} bar, and 4.5×10^{-2} to 2.9 at 1.67×10^{-2} bar. Results are shown in Figure 18, in which δ^{26}Mg and δ^{25}Mg of the droplet are plotted against the fraction of ^{24}Mg evaporated at each value of P_H^{tot}, and compared with the Rayleigh fractionation curve. The curves for evaporation into ambient gas depart from the Rayleigh fractionation curve by amounts which increase with increasing fraction of ^{24}Mg lost. As expected, at a constant fraction of ^{24}Mg evaporated, both δ^{26}Mg and δ^{25}Mg fall further and further below the values expected for Rayleigh fractionation as P_H^{tot} and thus $P_{Mg}^{amb}/P_{Mg}^{vap}$ increases. Because the initial evaporation rate of ^{24}Mg is greater than that of ^{25}Mg, the vapor pressure of ^{24}Mg decreases faster and the ambient pressure of ^{24}Mg increases faster than those of ^{25}Mg, causing reduction of the net loss rate of ^{24}Mg relative to that of ^{25}Mg. This produces a higher ^{25}Mg/^{24}Mg ratio in the instantaneous gas and a lower ^{25}Mg/^{24}Mg ratio in the residue at every stage of the evaporation process, in accordance with Eqn. 17, than during vacuum evaporation, described by Rayleigh fraction-

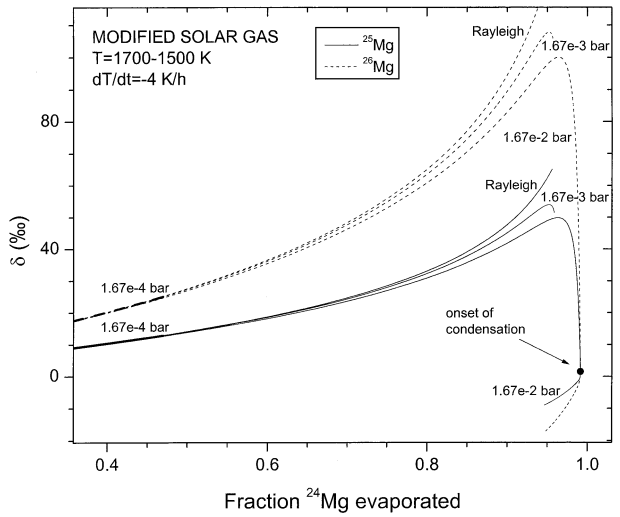

Fig. 18. Dependence of δ^{26}Mg and δ^{25}Mg of the liquid on fraction of ^{24}Mg evaporated from a droplet of composition δ and initial radius 0.25 cm during evaporation into a modified solar gas at $P_H^{tot} = 1.67 \times 10^{-2}$, 1.67×10^{-3} and 1.67×10^{-4} bar while cooling from 1700 to 1500 K at 4 K/h, compared with a Rayleigh fractionation curve for vacuum evaporation. Condensation occurs in the 1.67×10^{-2} bar case, and the fraction of ^{24}Mg evaporated at which this begins is marked on the curve for this P_H^{tot}.

ation. The curve for 1.67×10^{-4} bar is almost indistinguishable from the Rayleigh curve because $P_{Mg}^{amb}/P_{Mg}^{vap}$ is relatively small and because only ~47% of the Mg evaporates by 1500 K. At 1.67×10^{-3} bar, δ^{25}Mg and δ^{26}Mg reach maxima at 1548 K and decline thereafter, as seen previously for δ^{25}Mg in Figure 15. At 1.67×10^{-2} bar, δ^{25}Mg and δ^{26}Mg reach their maxima at ~1672 K where 96% of the ^{24}Mg has evaporated and, below this temperature, they fall precipitously, both in an absolute sense and relative to their values on the Rayleigh curves for this fraction of ^{24}Mg evaporated. The beginning of Mg condensation at 1649 K is marked by a maximum in the fraction of ^{24}Mg evaporated.

As a result of evaporation of Mg from a droplet into an ambient, Mg-containing gas, δ^{25}Mg and δ^{26}Mg in the residue depart by different amounts from a Rayleigh fractionation curve. The form of Eqn. 17 also suggests that the ratio of δ^{25}Mg to δ^{26}Mg expected from Rayleigh fractionation may not be preserved in this process. Even in a Rayleigh fractionation process, there is significant curvature on a plot of δ^{25}Mg vs. δ^{26}Mg. Because of this, departure of δ^{25}Mg from what is expected from Rayleigh fractionation is computed by multiplying δ^{26}Mg calculated at any temperature step by the δ^{25}Mg/δ^{26}Mg ratio of the Rayleigh fractionation curve at that δ^{25}Mg, and subtracting the result from δ^{25}Mg calculated at the same temperature step. This departure, Δ^{25}Mg, is plotted against δ^{25}Mg in Figure 19a for each of the evaporation calculations illustrated in Figure 18. The departure of δ^{26}Mg from what is expected from Rayleigh fractionation, Δ^{26}Mg, is computed in an analogous way from calculated values of δ^{25}Mg, and plotted against the latter in Figure 19b. At 1.67×10^{-4} bar, Δ^{25}Mg is a negative number which gradually becomes algebraically smaller with increasing δ^{25}Mg. At 1.67×10^{-3} bar, Δ^{25}Mg decreases more rapidly with δ^{25}Mg as the latter reaches its

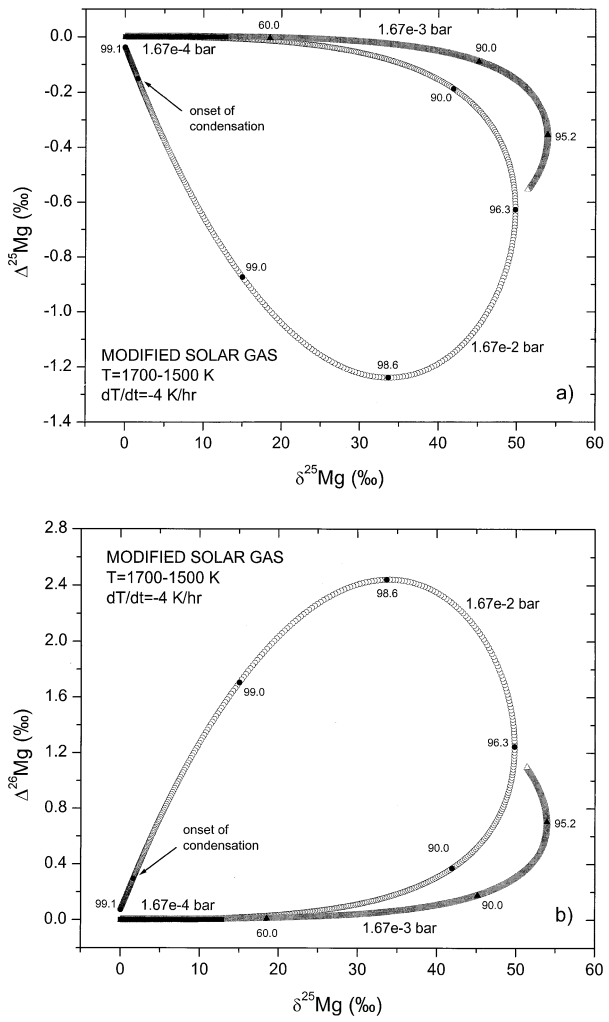

Fig. 19. Deviation of calculated (a) δ^{25}Mg and (b) δ^{26}Mg from that expected for Rayleigh fractionation for a droplet of composition δ and initial radius 0.25 cm evaporating into a modified solar gas at $P_H^{tot} = 1.67 \times 10^{-2}$, 1.67×10^{-3} and 1.67×10^{-4} bar while cooling from 1700 to 1500 K at 4 K/h, plotted against calculated δ^{25}Mg. Data points along the curves give the fraction of initial ^{24}Mg evaporated at various δ^{25}Mg values.

maximum, and continues to decrease rapidly as δ^{25}Mg decreases. At 1.67×10^{-2} bar, the absolute value of Δ^{25}Mg reaches a maximum at 1.24‰ after δ^{25}Mg reaches its maximum, declines rapidly with continued evaporation, and continues its decline after the onset of condensation. In the last temperature step before δ^{25}Mg becomes negative, 0.044% of the total Mg is in the droplet, and its Δ^{25}Mg is −0.04‰. Recall that the uncertainty in computing δ^{25}Mg is $<10^{-2}$‰, more than two orders of magnitude smaller than the maximum Δ^{25}Mg. Departures from Rayleigh fractionation are thus very small for relatively small fractions of ^{24}Mg evaporated but become much larger for greater degrees of Mg loss. This suggests that obtaining very precise measurements of both δ^{26}Mg and δ^{25}Mg may be a way of distinguishing lightly from heavily evaporated samples that end up with similar bulk chemical and isotopic compositions.

Unlike the case for magnesium isotopes, the gas/liquid par-

tition coefficient for silicon is the product of kinetic and equilibrium isotope fractionation factors, the latter of which is a function of temperature. This complication makes calculation of a reference Rayleigh fractionation curve dependent on cooling rate. Thus, while non-Rayleigh effects of the same sign as but ~10 times smaller than those seen for magnesium isotopes would be expected for silicon, no quantitative estimate is attempted here.

4. CONCLUSIONS

When a solid assemblage having the composition of a calculated high-temperature condensate is heated and melted in modified solar gas, i.e., its complementary vapor, vapor pressures of all species are almost identical to those when the ambient gas is pure $H_{2(g)}$, as the oxygen fugacity is only slightly higher in modified solar gas. Because the loss rate of Mg is greater than that of Si, the vapor pressure of $Mg_{(g)}$ falls and its ambient pressure rises faster than those of $SiO_{(g)}$ during isothermal evaporation, causing the net flux of $Mg_{(g)}$ to approach zero faster and MgO to approach its equilibrium concentration sooner than SiO_2. As time passes, δ^{25}Mg and δ^{29}Si increase in the droplet and decrease in the ambient gas. The net flux of each isotope crossing the droplet/gas interface is the difference between its outgoing and incoming flux. δ^{25}Mg and δ^{29}Si of this instantaneous gas become higher, first overtaking their values in the ambient gas, causing them to increase with time, and later overtaking their values in the droplet itself, causing them to decrease with time. When evaporation is complete enough to cause MgO to approach its equilibrium concentration, δ^{25}Mg of the droplet approaches that of the ambient gas. When this happens for SiO_2, the difference in δ^{29}Si between the droplet and the ambient gas approaches the value expected from the equilibrium gas/liquid fractionation factor for the assumed temperature. If the system is cooling while the droplet evaporates and if mass transfer ceases at the solidus temperature, 1500 K, the final MgO and SiO_2 contents of the droplet are slightly higher in modified solar gas than in pure $H_{2(g)}$, and the difference increases with increasing P_H^{tot} and decreasing cooling rate. During cooling under some conditions, net fluxes of evaporating species may become negative, causing reversal of the evaporation process into a condensation process, an increase in the MgO and/or SiO_2 content of the droplet with time, and an increase in their final concentrations with increasing P_H^{tot} and/or dust/gas ratio. At cooling rates $<\sim$3 K/h, closed-system evaporation at $P_H^{tot} \sim 10^{-3}$ bar in a modified solar gas, or at lower pressure in systems with enhanced dust/gas ratio, can yield the same δ^{25}Mg in a residual CMAS droplet for vastly different evaporated fractions of Mg. The δ^{25}Mg of a refractory residue by itself may thus be insufficient to determine the extent of Mg loss from its precursor, but combining this information with the isotopic composition of another element having a significantly different isotopic response to evaporation, such as Si, can be constraining. Evaporation of Mg into an Mg-bearing ambient gas causes δ^{26}Mg and δ^{25}Mg of the residual droplet to fall below the values expected from Rayleigh fractionation for the amount of ^{24}Mg evaporated, with the degree of departure increasing progressively with increasing ambient pressure of Mg relative to its vapor pressure and with increasing fraction evaporated. δ^{26}Mg and δ^{25}Mg do not depart proportionately from Rayleigh fractionation curves, with δ^{25}Mg being less than expected on the basis of δ^{26}Mg by up to ~1.2‰. Such departures from Rayleigh fractionation could be used in principle to distinguish heavily from lightly evaporated residues with the same δ^{25}Mg.

Acknowledgments—This work benefitted greatly from discussions with A. Campbell, R. N. Clayton, M. Humayun and S. B. Simon. We thank S. Tachibana and an anonymous referee for helpful reviews. We gratefully acknowledge support of the National Aeronautics and Space Administration through grant NAG5-4476.

Associate editor: U. Ott

REFERENCES

Anders E. and Grevesse N. (1989) Abundances of the elements: Meteoritic and solar. *Geochim. Cosmochim. Acta* **53**, 197–214.

Berman R. G. (1983) A Thermodynamic Model for Multicomponent Melts, With Application to the System CaO-MgO-Al_2O_3-SiO_2. Ph.D. dissertation, University of British Columbia.

Clayton R. N., Mayeda T. K., and Epstein S.(1978) Isotopic fractionation of silicon in Allende inclusions. In *Proc. 9th Lunar Planet. Sci. Conf.*, pp. 1267–1278.

Craig H., Gordon L. I., and Horibe Y. (1963) Isotopic exchange effects in the evaporation of water. 1. Low-temperature experimental results. *J. Geophys. Res.* **68**, 5079–5087.

Ebel D. S. and Grossman L. (2000) Condensation in dust-enriched systems. *Geochim. Cosmochim. Acta* **64**, 339–366.

Fedkin A. V., Grossman L., and Simon S. B. (2002) Evaporation of CAI liquids into solar gas. *Meteoritics Planet. Sci.* **37**, A45.

Grossman L., Ebel D. S., Simon S. B., Davis A. M., Richter F. M., and Parsad N. M. (2000) Major element chemical and isotopic compositions of refractory inclusions in C3 chondrites: The separate roles of condensation and evaporation. *Geochim. Cosmochim. Acta* **64**, 2879–2894.

Grossman L., Ebel D. S., and Simon S. B. (2002) Formation of refractory inclusions by evaporation of condensate precursors. *Geochim. Cosmochim. Acta* **66**, 145–161.

Humayun M. and Cassen P. (2000) Processes determining the volatile abundances of the meteorites and terrestrial planets. In *Origin of the Earth and Moon* (eds. R. M. Canup and K. Righter), pp. 3–23. University of Arizona Press, Tucson.

Lange R. A. and Carmichael I. S. E. (1987) Densities of Na_2O-K_2O-CaO-MgO-FeO-Fe_2O_3-Al_2O_3-TiO_2-SiO_2 liquids: New measurements and derived partial molar properties. *Geochim. Cosmochim. Acta* **51**, 2931–2946.

Lloyd R. M. (1966) Oxygen isotope enrichment of sea water by evaporation. *Geochim. Cosmochim. Acta* **30**, 801–814.

MacPherson G. J., Paque J. M., Stolper E., and Grossman L. (1984) The origin and significance of reverse zoning in melilite from Allende Type B inclusions. *J. Geol.* **92**, 289–305.

Ozawa K. and Nagahara H. (2001) Chemical and isotopic fractionations by evaporation and their cosmochemical implications. *Geochim. Cosmochim. Acta* **65**, 2171–2199.

Tsuchiyama A., Tachibana S., and Takahashi T. (1999) Evaporation of forsterite in the primordial solar nebula; rates and accompanied isotopic fractionation. *Geochim. Cosmochim. Acta* **63**, 2451–2466.